iScience

Article

Astrocytic FABP5 mediates retrograde endocannabinoid transport at central synapses

Graphical abstract

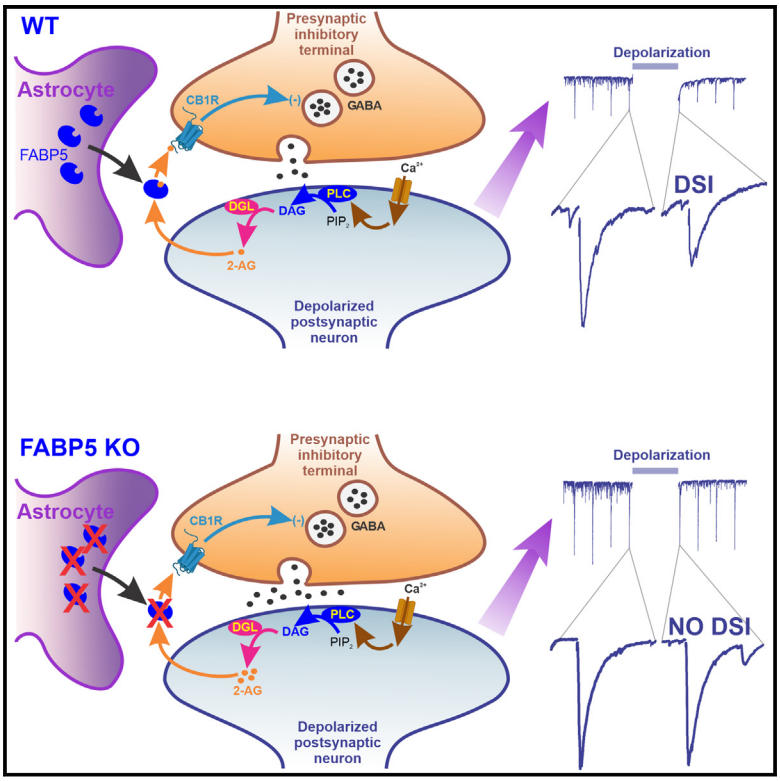

Highlights

- FABP5 is essential for retrograde 2-AG signaling at hippocampal synapses
- Extracellular FABP5 retains 2-AG binding capacity and mediates its synaptic transport
- The non-secreted FABP7 cannot rescue 2-AG signaling in the absence of FABP5
- Synaptic 2-AG transport requires astrocytic but not neuronal FABP5

Authors

Saida Oubraim, Mohammad Fauzan, Keith Studholme, ..., Iwao Ojima, Martin Kaczocha, Samir Haj-Dahmane

Correspondence

martin.kaczocha@stonybrook.edu (M.K.), sh38@buffalo.edu (S.H.-D.)

In brief

Neuroscience; Cellular neuroscience; Cell biology; Specialized functions of cells

Oubraim et al., 2025, iScience *28*, 112342
May 16, 2025
https://doi.org/10.1016/j.isci.2025.112342

CellPress

iScience

CellPress
OPEN ACCESS

Article

Astrocytic FABP5 mediates retrograde endocannabinoid transport at central synapses

Saida Oubraim,[1,9] Mohammad Fauzan,[2,3,9] Keith Studholme,[2] Chris Gordon,[2] Sherrye T. Glaser,[4] Roh-Yu Shen,[1,5] Iwao Ojima,[6,7] Martin Kaczocha,[2,3,7,8,10,*] and Samir Haj-Dahmane[1,5,10,11,*]

[1]Department of Pharmacology and Toxicology, Jacobs School of Medicine and Biomedical Sciences, University at Buffalo, State University of New York, Buffalo, NY, USA
[2]Department of Anesthesiology, Renaissance School of Medicine, Stony Brook University, Stony Brook, NY, USA
[3]Department of Biochemistry and Cell Biology, Stony Brook University, Stony Brook, NY, USA
[4]Department of Biological Sciences, Kingsborough Community College, Brooklyn, NY, USA
[5]University at Buffalo Neuroscience Program, Jacobs School of Medicine and Biomedical Sciences, University at Buffalo, State University of New York, Buffalo, NY, USA
[6]Department of Chemistry, Stony Brook University, Stony Brook, NY, USA
[7]Institute of Chemical Biology and Drug Discovery, Stony Brook University, Stony Brook, NY, USA
[8]Stony Brook University Pain and Analgesia Research Center (SPARC), Renaissance School of Medicine, Stony Brook University, Stony Brook, NY, USA
[9]These authors contributed equally
[10]These authors contributed equally
[11]Lead contact
*Correspondence: martin.kaczocha@stonybrook.edu (M.K.), sh38@buffalo.edu (S.H.-D.)
https://doi.org/10.1016/j.isci.2025.112342

SUMMARY

Endocannabinoids (eCBs) regulate synaptic function via cannabinoid receptors. While eCB signaling is well understood, the mechanisms underlying eCB synaptic transport are poorly characterized. Using 2-arachidonoylglycerol (2-AG)-mediated depolarization-induced suppression of inhibition (DSI) in the hippocampus as a readout of retrograde eCB signaling, we demonstrate that the deletion of fatty acid binding protein 5 (FABP5) impairs DSI. In FABP5 KO mice, DSI was rescued by re-expressing wild-type FABP5 but not an FABP5 mutant that does not bind 2-AG. Importantly, the deletion of astrocytic FABP5 blunted DSI, which was rescued by its re-expression in the astrocytes of FABP5 KO mice. Neuronal FABP5 was dispensable for 2-AG signaling. DSI was also rescued by expressing a secreted FABP5 variant but not by FABP7, an astrocytic FABP that does not undergo secretion. Our results demonstrate that extracellular FABP5 of astrocytic origin controls 2-AG transport and that FABP5 is adapted to coordinate intracellular and synaptic eCB transport.

INTRODUCTION

The endocannabinoids (eCBs) 2-arachidonoylglycerol (2-AG) and anandamide (AEA) function as endogenous lipid agonists at cannabinoid receptors and regulate an array of behavioral and physiological functions.[1–3] Canonically, eCBs are synthesized and released from postsynaptic neurons in response to neuronal activation and act as retrograde messengers by activating presynaptic cannabinoid receptor 1 (CB1R) to dampen synaptic transmission. In addition, eCBs can interact with a diverse array of receptors, including cannabinoid receptor 2 (CB2R), G protein-coupled receptor 55 (GPR55), transient receptor potential vanilloid 1 (TRPV1), and peroxisome proliferator-activated receptors (PPARs).[4–7] The activation of CB1R by 2-AG mediates various forms of synaptic plasticity, including depolarization-induced suppression of inhibition (DSI) and excitation (DSE), first reported at hippocampal CA1 GABA synapses and cerebellar glutamate synapses, respectively.[8–11] The magnitude and duration of 2-AG signaling is governed predominantly by diacylglycerol lipase alpha (DAGLα)-mediated biosynthesis in postsynaptic neurons and subsequent inactivation by monoacylglycerol lipase (MAGL) in presynaptic terminals and surrounding astrocytes.[11–16] In contrast to hydrophilic neurotransmitters, the lipophilicity of eCBs limits their diffusion across an aqueous milieu.[17–23] Consequently, the spatial separation between 2-AG biosynthesis in postsynaptic neurons and CB1R on presynaptic terminals, combined with the rapid onset of 2-AG-mediated short-term synaptic plasticity, necessitates a mechanism(s) enabling efficient trafficking of 2-AG across the synaptic cleft.[8,24]

Fatty acid binding proteins (FABPs) are a family of proteins that bind diverse lipid species and mediate their intracellular trafficking.[25–28] Among the FABPs, FABP3, FABP5, and FABP7 are expressed in the brain and regulate distinct and non-overlapping physiological functions.[29–34] While all three FABPs bind AEA and 2-AG with varying affinities, previous work has established that FABP5 is a major intracellular carrier of eCBs *in vitro* and *in vivo*.[19,24,35–39] In addition, we recently demonstrated that

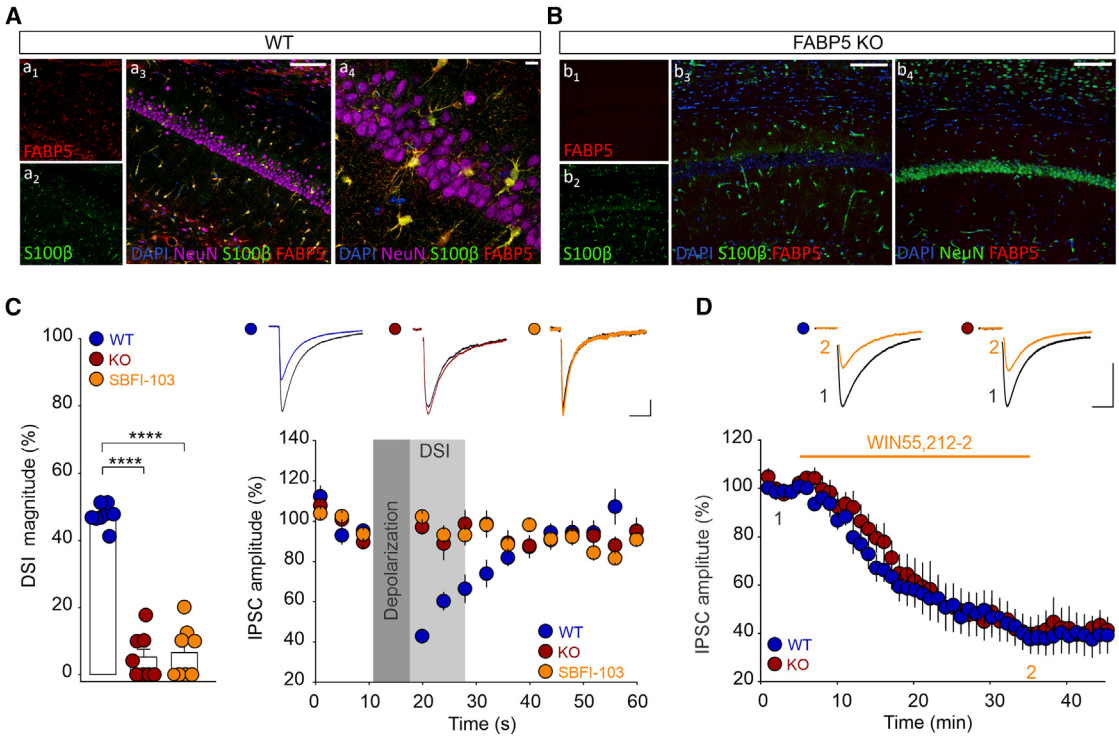

Figure 1. FABP5 is essential for 2-AG-mediated DSI at CA1 GABA synapses

(A) Immunolabelling of FABP5 expression in the hippocampal CA1 region of WT mice. a_1-a_2, Labeling of FABP5 and the astrocyte marker s100β. a_3, Triple labeling between the neuronal marker NeuN, FABP5, and s100β. Note the robust colocalization of FABP5 with s100β. Scale bar: 100 μm. a_4, Higher magnification of NeuN, FABP5 and s100β triple labeling. Scale bar: 10 μm.

(B) Lack of FABP5 immunostaining in the hippocampus of FABP5 KO mice. b_1, b_2, FABP5 and s100β staining. b_3, Merged image of FABP5, s100β, and DAPI labeling. Scale bar: 100 μm. b_4, merged image of FABP5, NeuN, and DAPI labeling. Scale bar: 100 μm.

(C) Inhibition of FABP5 blunts hippocampal DSI. Left panel illustrates averaged magnitude of DSI obtained in WT (●: 47.41 ± 1.11%; n = 8 cells; N = 3 mice), FABP5 KO (●: 5.26 ± 2.37%; n = 8 cells; N = 3 mice; $p = 1.95 \times 10^{-11}$ versus WT), and following FABP5 inhibition with 10 μM SBFI-103 (●: 6.59 ± 2.72%; n = 8 cells; N = 3 mice; $p = 3.59 \times 10^{-11}$ versus WT). Upper right panel depicts representative traces of IPSCs recorded before and during DSI. Scale bars: 100 ms, 200 pA. Lower right panel represents the time course of DSI.

(D) Deletion of FABP5 does not alter the function of CB1Rs. Upper panel illustrates representative IPSCs traces collected before (1) and during the application of WIN55,212-2 (10 μM) (2) from WT (●) and KO (●). Lower panel is a summary of the depression of IPSC amplitude induced by WIN55,212-2 in WT (●: 42.53 ± 6.88%; n = 7 cells; N = 3 mice; $p = 1.75 \times 10^{-7}$ versus baseline) and KO (●: 43.01 ± 7.24%; n = 7 cells; N = 3 mice; $p = 1.44 \times 10^{-7}$ versus baseline). Scale bars: 50 ms, 50 pA. Data are represented as mean ± SEM. ****$p < 0.001$. one-way ANOVA with Bonferroni's multiple comparisons test.

FABP5 is essential for retrograde 2-AG signaling at glutamate synapses in the dorsal raphe nucleus and at striatal GABA synapses.[40,41]

FABP5 is expressed in neurons and astrocytes in various brain areas, albeit with predominant expression in astrocytes.[31,40–42] Mounting evidence indicates that subsets of FABPs can be secreted from cells through unconventional mechanisms,[43–46] suggesting that FABPs may also serve as extracellular carriers for bioactive lipids, including eCBs. Consistent with this notion, FABP5 was identified as a component of the astrocyte-neuron synaptic proteome,[47] providing anatomical evidence that extracellular FABP5 may serve as a synaptic carrier for 2-AG. In this study, we combined the cell-type specific modulation of FABP5 expression with engineered FABP5 variants to delineate the cellular source(s) and contributions of extracellular and intracellular FABP5 in mediating 2-AG transport. Employing 2-AG mediated DSI at hippocampal GABA synapses,[8–11] we establish that secreted astrocytic FABP5 orchestrates retrograde 2-AG signaling, thereby elucidating the mechanism underlying eCB transport at central synapses.

RESULTS

Fatty acid binding protein 5 is essential for retrograde 2-arachidonoylglycerol signaling at hippocampal GABA synapses

We first profiled the expression of FABP5 in the CA1 region of the hippocampus using a validated antibody,[40,41,48–51] which revealed that FABP5 was robustly expressed in this region and was mainly distributed in astrocytes (92.7 ± 0.5% of astrocytes and 1.6 ± 0.3% of neurons) (Figure 1A, Videos S1 and S2). As expected, FABP5 labeling was absent in the hippocampus of FABP5 KO mice (Figure 1B). Pharmacological inhibition of FABP5 using the selective inhibitor SBFI-103[50,52,53] markedly suppressed the magnitude of DSI in WT mice (Figure 1C). Similar results were observed in FABP5 KO mice (Figure 1C). This

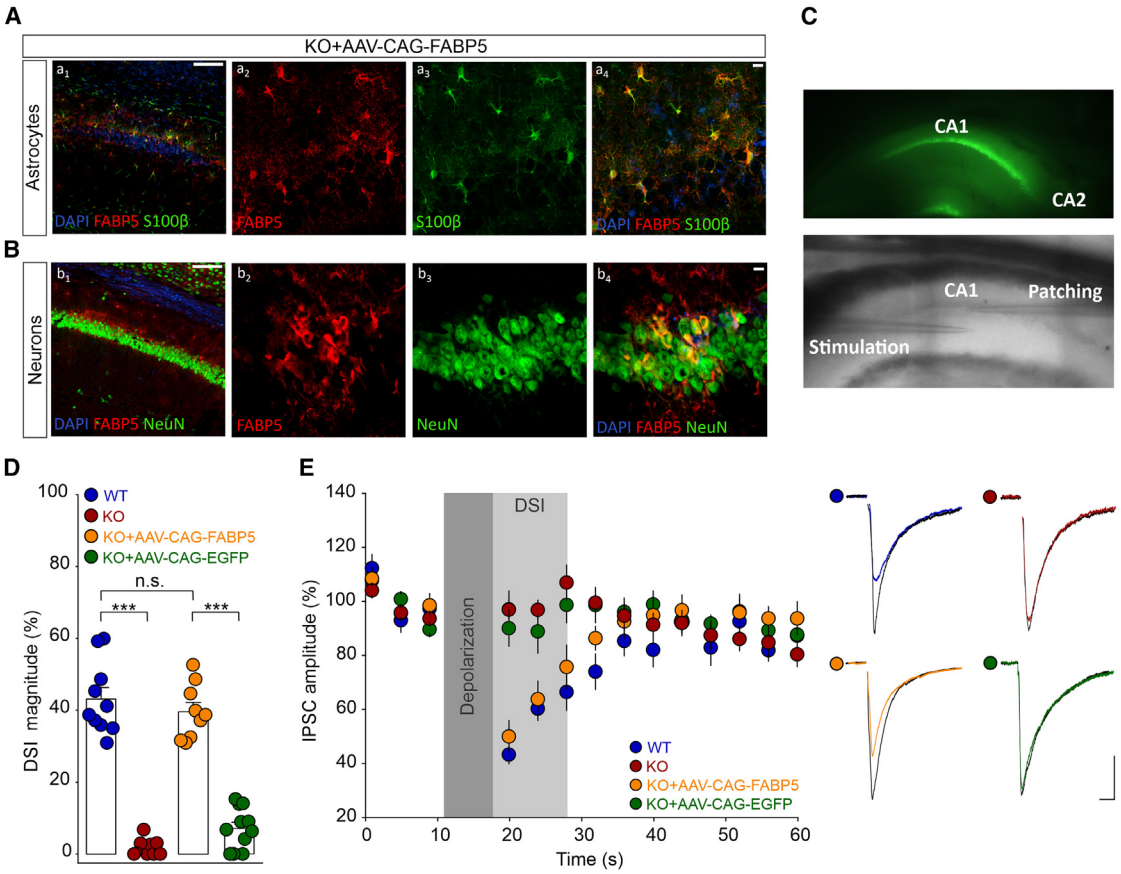

Figure 2. Expression of FABP5 in FABP5 KO mice restores hippocampal DSI

(A) AAV-mediated expression of FABP5 in astrocytes of the hippocampal CA1 region of FABP5 KO mice. a_1, Low magnification image of FABP5, DAPI, and s100β labeling. Scale bar: 100 μm. a_2-a_4, High magnification labeling of FABP5, s100β, and merge. Scale bar: 10 μm.

(B) AAV-mediated expression of FABP5 in neurons of FABP5 KO mice. b_1, Low magnification labeling of DAPI, NeuN, and FABP5. Scale bar: 100 μm. b_2-b_4, High magnification labeling of FABP5, NeuN, and merge with DAPI. Scale bars: 10 μm.

(C) Upper image illustrates GFP expression in the CA1 region. Lower image shows recording and stimulating electrodes in the same CA1 region expressing FABP5.

(D) Re-expression of FABP5 restores DSI in FABP5 KO mice. D_1, Averaged magnitude of the DSI in WT (●: 43.18 ± 3.16%; $n = 10$ cells; $N = 3$ mice), KO (●: 1.76 ± 0.76%; $n = 9$ cells; $N = 3$ mice; $p = 5.96 \times 10^{-14}$ versus WT), KO+AAV-CAG-FABP5 (●: 39.63 ± 2.55%; $n = 9$ cells; $N = 3$ mice; $p = 1$ versus WT), and KO+AAV-CAG-EGFP (●: 7.15 ± 1.73%; $n = 11$ cells; $N = 4$ mice; $p = 2.75 \times 10^{-11}$ versus KO+AAV-CAG-FABP5). D_2, Summary graph of the time course of the DSI obtained in WT (●), KO (●), KO+AAV-CAG-FABP5 (●), and KO+AAV-CAG-EGFP (●). D_3, Representative traces of IPSCs recorded before and during DSI from WT (●), KO (●), KO+AAV-CAG-FABP5 (●), and KO+AAV-CAG-EGFP (●). Scale bars: 50 ms, 200 pA. Data are represented as mean ± SEM. ***$p < 0.001$, one-way ANOVA, with Bonferroni's multiple comparisons test.

impairment of DSI was not mediated by a dysfunction of CB1R as the synthetic CB1R agonist WIN55,212-2 induced comparable depression of GABAA-mediated IPSCs in WT and FABP5 KO mice (Figure 1D). Moreover, the expression of CB1R and the enzymes mediating 2-AG biosynthesis and catabolism was not altered in FABP5 KO mice compared to WT littermates, while 2-AG levels were elevated (Figures S1A–S1C). Next, we examined whether the re-expression of FABP5 in the hippocampus of FABP5 KO mice could rescue 2-AG signaling. Indeed, the injection of AAV-CAG-FABP5 induced robust FABP5 expression in the CA1 region of the hippocampus (Figures 2A and 2B) and fully restored DSI, while a control AAV was without effect (Figures 2D and 2E). These results indicate that the blockade of DSI following FABP5 inhibition cannot be attributed to impaired 2-AG biosynthesis, CB1R dysfunction, or compensatory adaptations in FABP5 KO mice.

To establish that 2-AG transport by FABP5 is required for the rescue of DSI, we engineered an FABP5 variant (termed $FABP5^{MUT}$) harboring mutations in key residues (R109A, R129A, Y131A) within the FABP5 binding pocket that mediates ligand interactions (Figure S2A).[37,54] As expected, purified $FABP5^{MUT}$ lacked binding affinity for 2-AG and the related lipid arachidonic acid (Figures S2B and S2C). Importantly, the AAV-mediated expression of $FABP5^{MUT}$ in the hippocampus of FABP5 KO mice failed to rescue DSI and did not alter the WIN55,212-2 induced depression of IPSC amplitudes (Figures 3A–3D). Moreover, the expression of $FABP5^{MUT}$ in WT mice had no effect on the magnitude or kinetics of DSI, confirming

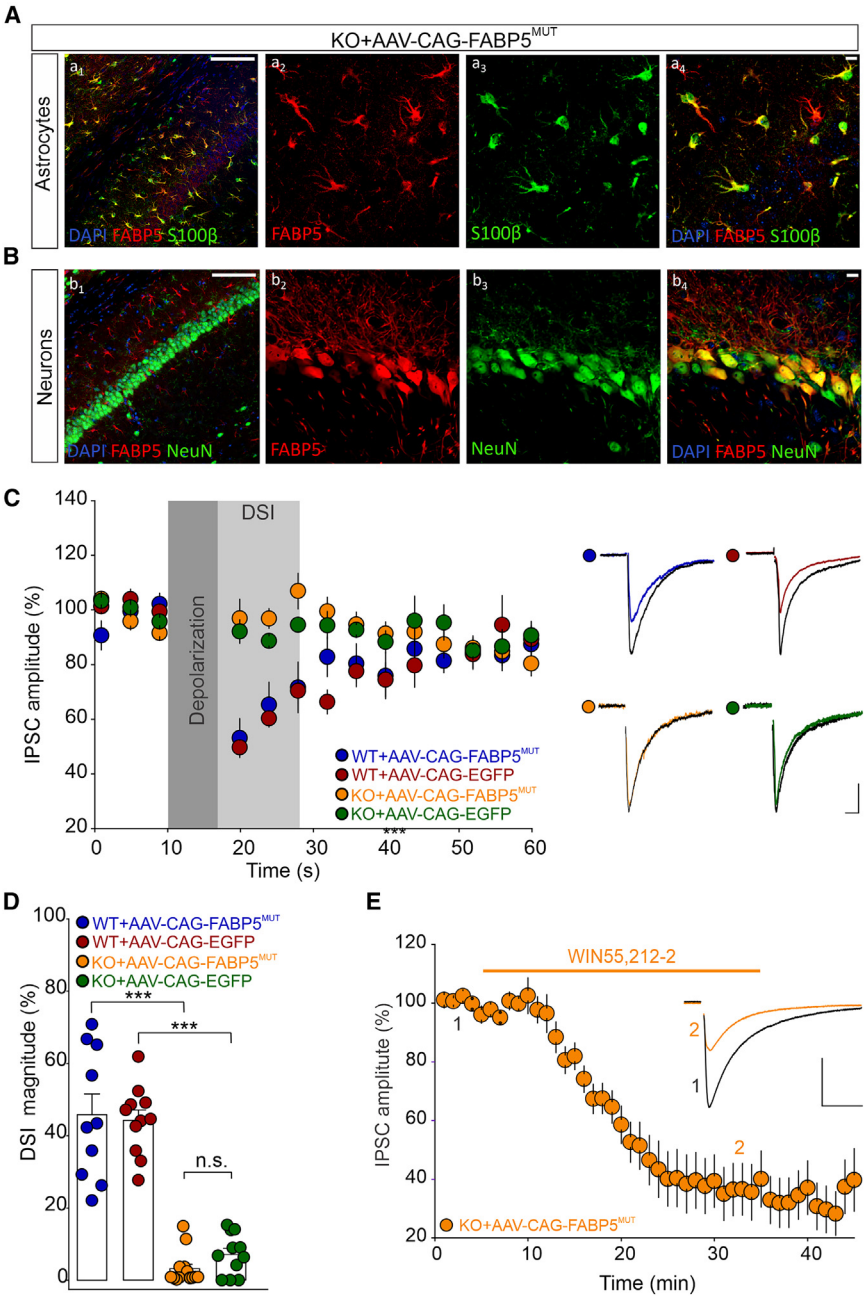

Figure 3. FABP5^{MUT} fails to rescue hippocampal DSI in FABP5 KO mice

(A) Astrocytic expression of FABP5^{MUT} in the CA1 region of FABP5 KO mice. a_1, Low magnification image of FABP5, s100β, and DAPI labeling in the CA1 region. Scale bar: 100 μm. a_2-a_4, High magnification immunostaining of FABP5 labeling, s100β, and merge. Scale bar: 10 μm.

(B) Neuronal expression of FABP5^{MUT} in the CA1 region of FABP5 KO mice. b_1, Low magnification image of FABP5, NeuN, and DAPI labeling in the CA1 region. Scale bar: 100 μm. b_2-b_4, High magnification immunostaining of FABP5, NeuN, and merge with DAPI. Scale bar: 10 μm.

(C) Expression of FABP5^{MUT} in FABP5 KO mice did not rescue hippocampal DSI. Left panel, summary of time course of DSI recorded from wild-type WT+AAV-CAG-FABP5^{MUT} (●), WT+AAV-CAG-EGFP (●), KO+AAV-CAG-FABP5^{MUT} (●), and KO+AAV-CAG-EGFP (●). Right panel, Sample superimposed IPSC traces collected before and during the DSI. Scale bars: 50 ms, 200 pA

(D) Summary of DSI magnitude obtained in WT+AAV-CAG-FABP5^{MUT} (●: 45.86 ± 5.67%; n = 10 cells; N = 3 mice), WT+AAV-CAG-EGFP (●: 44.28 ± 2.86%; n = 11 cells; N = 3 mice), KO+AAV-CAG-FABP5^{MUT} (●: 3.19 ± 1.27%; n = 13 cells; N = 3 mice; $p = 1.54\times10^{-11}$ versus WT+AAV-CAG-FABP5^{MUT}), KO+AAV-CAG-EGFP (●: 7.15 ± 1.73%; n = 11 cells; N = 3 mice; p = 1 versus KO+AAV-CAG-FABP5^{MUT}, $p = 1.05\times10^{-9}$ versus WT+AAV-CAG-EGFP.

(E) Expression of FABP5^{MUT} in FABP5 KO mice does not affect the depression of IPSC amplitude induced by WIN55,212-2 (10 μM) (●, 34.75 ± 68.28%; n = 7; $p = 2.21\times10^{-4}$ versus baseline). Inset, Sample IPSCs traces collected before and during the application of WIN55,212-2 (10μM). Scale bars: 25 ms, 50 pA. Data are represented as mean ± SEM. ***$p < 0.001$, one-way ANOVA with Bonferroni's multiple comparisons test, or paired sample t-test.

that this protein does not interfere with the function of native FABP5 (Figures 3C and 3D). Collectively, these results indicate that FABP5-mediated 2-AG transport is indispensable for the induction of DSI.

Extracellular fatty acid binding protein 5 mediates retrograde 2-arachidonoylglycerol signaling

Extensive work has established that FABP5 is an intracellular carrier for eCBs.[19,36–38] To shuttle 2-AG across the synaptic cleft, FABP5 must be secreted and retain its function within the extracellular space. We recently demonstrated that FABP5 is released by astrocytes[40] but it remains to be established whether an extracellular pool of FABP5 mediates synaptic 2-AG transport. Therefore, we designed a secreted FABP5 variant by fusing the signal peptide from Igκ to the N-terminus of FABP5 (termed FABP5^{SEC}). We transfected HEK293 cells and confirmed the secretion of FABP5^{SEC}, which was purified from the culture media (Figure S3). Purified FABP5^{SEC} retained its capacity to bind 2-AG, albeit with a slight loss of affinity compared to intracellular FABP5 (Figure 4A). The expression of FABP5^{SEC} in FABP5 KO mice fully restored DSI (Figures 4B–4D), indicating that extracellular FABP5 is sufficient for retrograde 2-AG signaling.

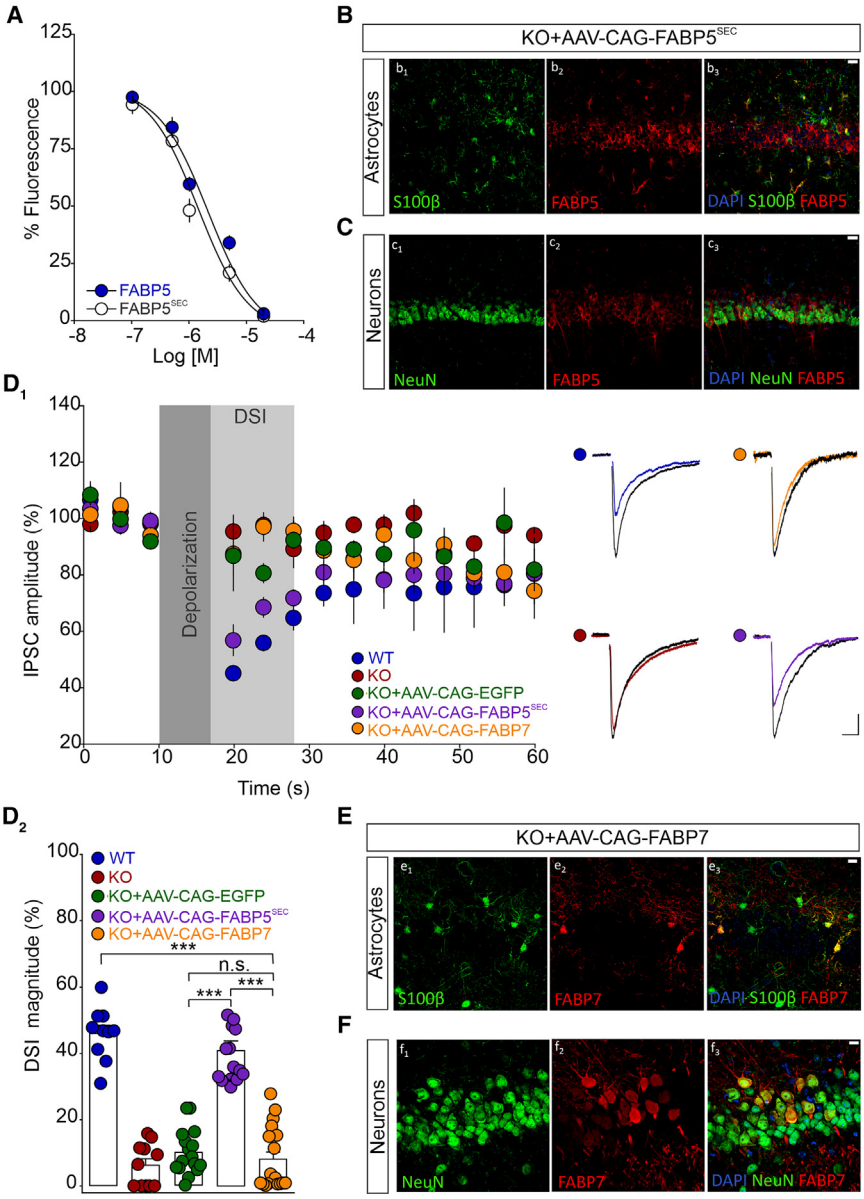

Figure 4. Extracellular pool of FABP5 mediates hippocampal DSI

(A) Secreted FABP5 variant (FABP5^{SEC}) binds to 2-AG with comparable affinity to WT FABP5 (FABP5 Ki: 1.0 ± 0.1 μM; FABP5^{SEC} Ki: 1.6 ± 0.2 μM, *n* = 4).

(B) AAV-mediated expression of FABP5^{SEC} in CA1 astrocytes of FABP5 KO mice. b_1-b_3, Immunolabelling for FABP5, s100β, and merge with DAPI. Scale bar: 10 μm.

(C) Neuronal expression of FABP5^{SEC} in the CA1 region. c_1-c_3, Immunolabelling for FABP5, NeuN, and merge with DAPI. Scale bar: 10 μm.

(D) Expression of FABP5^{SEC} but not FABP7 restores DSI in FABP5 KO mice. D_1, left panel, Summary of the time course of hippocampal DSI recorded from WT (●), KO (●), KO+AAV-CAG-EGFP (●), KO+AAV-CAG-FABP5^{SEC} (●), and KO+AAV-CAG-FABP7 (●). Right panel, Superimposed IPSC traces collected before and during DSI. D_2, Averaged magnitude of DSI obtained in WT (●: 45.99 ± 2.51%; *n* = 10 cells; *N* = 5 mice), KO (●: 5.85 ± 1.21%; *n* = 17 cells; *N* = 5 mice), KO+AAV-CAG-EGFP (●: 10.24 ± 1.70%; *n* = 16 cells; *N* = 5 mice), KO+AAV-CAG-FABP5^{SEC} (●: 38.61 ± 1.94%; *n* = 17 cells; *N* = 5 mice; $p = 9.83 \times 10^{-16}$ versus KO+AAV-CAG-EGFP, $p = 0.16$ vs. WT), and KO+AAV-CAG-FABP7 (●: 8.10 ± 2.19%; *n* = 18 cells; *N* = 5 mice; $p = 3.62 \times 10^{-19}$ versus WT, $p = 1$ versus KO+AAV-CAG-EGFP, $p = 8.22 \times 10^{-18}$ versus KO+AAV-CAG-FABP5^{SEC}). Scale bars: 100 ms, 200 pA

(E and F) Expression of FABP7 in the CA1 region of FABP5 KO mice. e_1-e_3, Immunolabelling for FABP7, s100β and merge. Scale bar: 10 μm. f_1-f_3, immunolabelling for FABP7, NeuN and merge. Scale bar: 10 μm. Data are represented as mean ± SEM. ***$p < 0.001$, one-way ANOVA with Bonferroni's multiple comparisons test.

Multiple unconventional pathways have been proposed to govern the cellular secretion of FABPs.[43–45] However, tools permitting selective blockade of FABP5 release via each of these pathways are currently lacking. To overcome this limitation and establish that an extracellular pool of FABP5 is necessary for 2-AG transport, we leveraged an alternate approach using FABP7, an astrocytic FABP that displays a high affinity for 2-AG but does not undergo secretion.[37,55] Strikingly, the AAV-mediated expression of FABP7 in the hippocampus of FABP5 KO mice failed to rescue the DSI (Figures 4D and 4E), supporting the notion that secreted FABP5 mediates the synaptic transport of 2-AG. To determine whether the conversion of FABP7 into a secreted variant could mimic the effects of FABP5^{SEC} and restore DSI, we engineered FABP7^{SEC} using the same approach as FABP5^{SEC} and purified the protein from the culture media of HEK293 cells (Figure S3). Unexpectedly, although FABP7^{SEC} was secreted from cells, it was nonfunctional, as evidenced by its inability to bind 2-AG and AA (Figure S3). These results indicate that FABP5 is endowed with the capacity to undergo cellular secretion while maintaining its function within the extracellular space, thereby enabling it to serve as a synaptic eCB carrier.

Astrocytic fatty acid binding protein 5 is necessary and sufficient for retrograde 2-arachidonoylglycerol signaling

Astrocytes robustly express and secrete FABP5 (Figure 1).[40] Based on this finding, we hypothesized that astrocytic FABP5 mediates the synaptic transport of 2-AG. To directly test this concept, we developed an FABP5^{FLOX} mouse that encodes an STOP-flox tdTomato reporter that is expressed following Cre-mediated FABP5 deletion (Figure 5A). We first confirmed that the FABP5^{FLOX} mice express FABP5, lack tdTomato labeling in the absence of Cre-mediated recombination, and exhibit robust

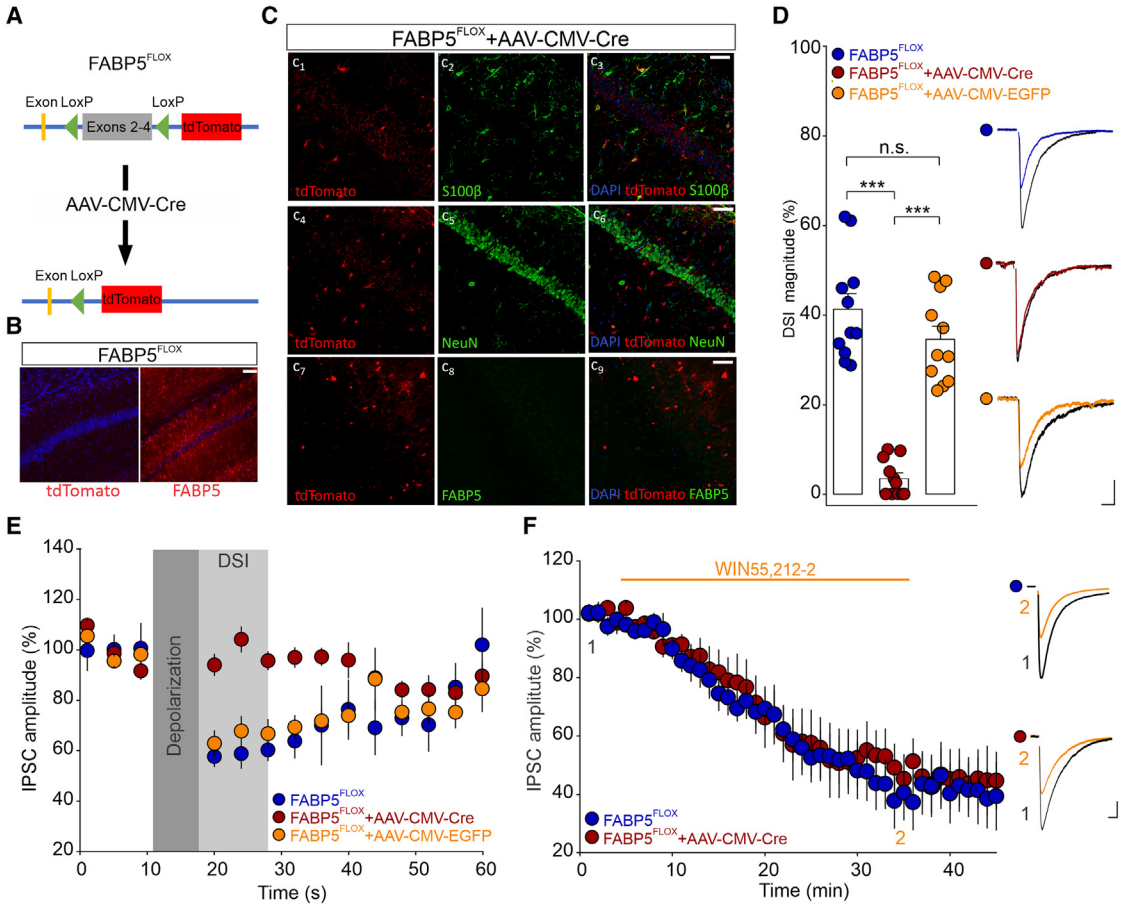

Figure 5. Conditional deletion of hippocampal FABP5 blunts DSI

(A) Schematic of the gene structure of FABP5^{FLOX} mice.

(B) Expression of FABP5 and a lack of tdTomato in the hippocampus of FABP5^{FLOX} mice. Left panel, Immunostaining for DAPI and tdTomato in CA1 region of FABP5^{FLOX} mice. Right panel, Immunostaining for DAPI and FABP5 in CA1 region of FABP5^{FLOX} mice. Scale bar: 50 μm.

(C) Cre-mediated deletion of FABP5 and expression of tdTomato in the CA1 region of FABP5^{FLOX} mice. c1-c3, Immunostaining for tdTomato, s100β, and merge. c4-c6, Immunolabeling of tdTomato, NeuN and merge. c7-c9, immunolabeling of tdTomato, FABP5 and merge. Scale bar: 50 μm.

(D) Conditional deletion of FABP5 inhibits DSI. Left panel, Averaged magnitude of hippocampal DSI recorded in FABP5^{FLOX} (●: 41.29 ± 3.54%; n = 11 cells; N = 5 mice), FABP5^{FLOX}+AAV-CMV-Cre (●: 3.51 ± 1.22%; n = 11 cells; N = 3 mice; $p = 3.95\times10^{-12}$ versus FABP5^{FLOX}), FABP5^{FLOX}+AAV-CMV-EGFP (●: 34.61 ± 2.93%; n = 11 cells; N = 4 mice; $p = 1.44\times10^{-9}$ versus FABP5^{FLOX}+AAV-CMV-Cre, p = 0.87 versus FABP5^{FLOX}). Right panel, representative traces of IPSCs collected before and during DSI from FABP5^{FLOX} (●), FABP5^{FLOX}+AAV-CMV-Cre (●), and FABP5^{FLOX}+AAV-CMV-EGFP (●). Scale bars: 100 ms, 200 pA

(E) Averaged time course of the DSI recorded in FABP5^{FLOX} and FABP5^{FLOX}+AAV-CMV-EGFP mice.

(F) Conditional deletion of FABP5 in the CA1 region does not affect the function of presynaptic CBRs. Left panel, Summary of the depression of IPSC amplitude induced by WIN55,212-2 (10 μM) in FABP5^{FLOX} (●: 46.13 ± 9.15%; n = 7 cells; N = 4 mice; $p = 7.03\times10^{-5}$ versus baseline) and FABP5^{FLOX}+AAV-CMV-Cre (●: 38.76 ± 9.63%; n = 6 cells; N = 4 mice; $p = 2.55\times10^{-5}$ versus baseline). Right panel, superimposed IPSCs traces collected before and during WIN55,212-2 application. Scale bars: 100 ms, 200 pA. Data are represented as mean ± SEM. ***p < 0.001, one-way ANOVA with Bonferroni's multiple comparisons test.

DSI, indicating that the mice exhibit normal retrograde 2-AG signaling (Figures 5B, 5D, and 5E). The injection of AAV-CAG-Cre resulted in FABP5 deletion, as evidenced by tdTomato expression and a concurrent loss of FABP5 immunoreactivity (Figure 5C). Conditional FABP5 deletion also resulted in a complete blockade of DSI without altering CB1R function, whereas the injection of a control AAV was without effect (Figures 5D–5F). These results indicate that the ablation of FABP5 in adult mice abolishes hippocampal retrograde 2-AG signaling.

To directly interrogate the contribution of astrocytic FABP5 to 2-AG transport, we conditionally deleted FABP5 in astrocytes by crossing FABP5^{FLOX} mice with the tamoxifen-inducible Aldh1l1-Cre/ERT2 line (Figure 6A).[56] Tamoxifen injection resulted in astrocyte-specific FABP5 deletion and concomitant tdTomato expression (Figure 6B). Strikingly, loss of astrocytic FABP5 led to a complete inhibition of DSI without the alteration of CB1R function (Figures 6C–6E). In contrast, DSI was unaffected following tamoxifen treatment in littermates lacking Cre. Next, we assessed whether astrocyte-specific FABP5 re-expression in the hippocampus of FABP5 KO mice is sufficient to rescue 2-AG signaling. Indeed, the expression of FABP5 under the control of the gfaABC1D promoter (AAV-gfaABC1D-FABP5-GFP)

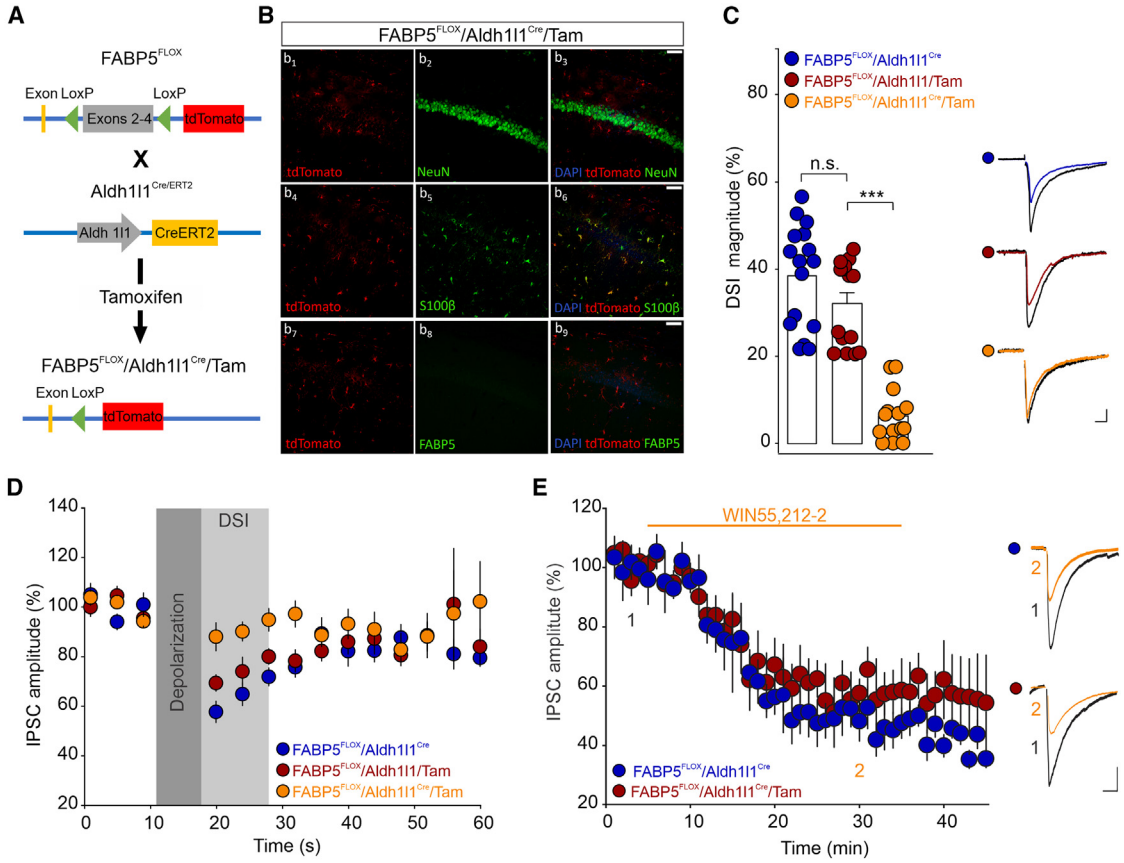

Figure 6. Deletion of astrocytic FABP5 impairs hippocampal DSI

(A) Schematic showing the experimental strategy used to delete astrocytic FABP5 and generate FABP5^{FLOX}/Aldh1l1^{Cre} mice. FABP5^{FLOX}/Aldh1l1^{Cre}/Tam represent tamoxifen-injected FABP5^{FLOX}/Aldh1l1^{Cre} mice, FABP5^{FLOX}/Aldh1l1/Tam represent tamoxifen-injected Cre^{-} littermates, while FABP5^{FLOX}/Aldh1l1^{Cre} mice received vehicle.

(B) Tamoxifen-induced deletion of the FABP5 and expression of tdTomato in astrocytes in the CA1 region of FABP5^{FLOX}/Aldh1l1^{Cre}/Tam mice. b1-b3, Images of tdTomato, NeuN staining, and merge. b4-b6, Images of tdTomato, s100β, and merge. b7-b9, images of immunostaining for tdTomato, FABP5, and merge. Note the expression of tdTomato in astrocytes but not in neurons and the absence of FABP5 expression. Scale bars: 50 μm.

(C) Tamoxifen-induced deletion of FABP5 impairs DSI in FABP5^{FLOX}/Aldh1l1^{Cre}/Tam mice. Left panel, Averaged DSI magnitude obtained in FABP5^{FLOX}/Aldh1l1^{Cre} (●: 38.12 ± 2.97%; n = 16 cells; N = 4 mice), in FABP5^{FLOX}/Aldh1l1/Tam (●: 32.12 ± 2.50%; n = 15 cells; N = 4 mice; p = 0.27 versus FABP5^{FLOX}/Aldh1l1^{Cre}) and in FABP5^{FLOX}/Aldh1l1^{Cre}/Tam (●: 6.32 ± 1.85%; n = 14 cells; N = 4 mice; $p = 2.22\times10^{-8}$ versus FABP5^{FLOX}/Aldh1l1/Tam). Right panel, Superimposed IPSC traces collected before and during DSI from FABP5^{FLOX}/Aldh1l1^{Cre} (●), FABP5^{FLOX}/Aldh1l1/Tam (●), and FABP5^{FLOX}/Aldh1l1^{Cre}/Tam (●) mice. Scale bars: 100 ms, 200 pA.

(D) Averaged time course of DSI recorded from FABP5^{FLOX}/Aldh1l1^{Cre} (●), FABP5^{FLOX}/Aldh1l1/Tam (●), and FABP5^{FLOX}/Aldh1l1^{Cre}/Tam (●) mice.

(E) Deletion of astrocytic FABP5 does not affect the function of CB1Rs. Summary of the depression of IPSC amplitude induced by WIN55,212-2 (10 μM) in FABP5^{FLOX}/Aldh1l1^{Cre} (●:44.75 ± 3.73%; n = 5 cells; N = 3 mice; $p = 2.52\times10^{-6}$ versus baseline) and FABP5^{FLOX}/Aldh1l1^{Cre}/Tam (●: 54.74 ± 8.11%; n = 5 cells; N = 3 mice; $p = 2.29\times10^{-5}$ versus baseline). Right panel, Sample IPSCs traces collected before and during WIN55,212-2 application. Scale bars: 100 ms, 100 pA. Data are represented as mean ± SEM. ***p < 0.001, one-way ANOVA with Bonferroni's multiple comparisons test.

resulted in astrocyte-selective FABP5 expression and full restoration of DSI (Figures 7A and 7B). A control AAV was without effect (Figure 7B).

We subsequently examined the role of neuronal FABP5 by injecting FABP5^{FLOX} mice with AAV-hSyn-Cre, which expresses Cre under the control of the neuron-specific synapsin I promoter. While AAV-hSyn-Cre resulted in robust neuronal transduction, as shown by GFP labeling (Figure S4), only sparse tdTomato signal was observed, consistent with the predominant expression of FABP5 in astrocytes (Figures 1A and S5A). Notably, the deletion of FABP5 had no effect on the magnitude of DSI (Figures S5B and S5C), indicating that neuronal FABP5 is dispensable for 2-AG retrograde signaling. Interestingly, the AAV-mediated re-expression of FABP5 in hippocampal neurons of FABP5 KO mice resulted in a small albeit significant DSI (Figures 7C and 7D), potentially reflecting FABP5 secretion following overexpression in neurons. Collectively, our results are the first to ascribe an essential function for astrocytic FABP5 as a synaptic 2-AG transport protein in the hippocampus.

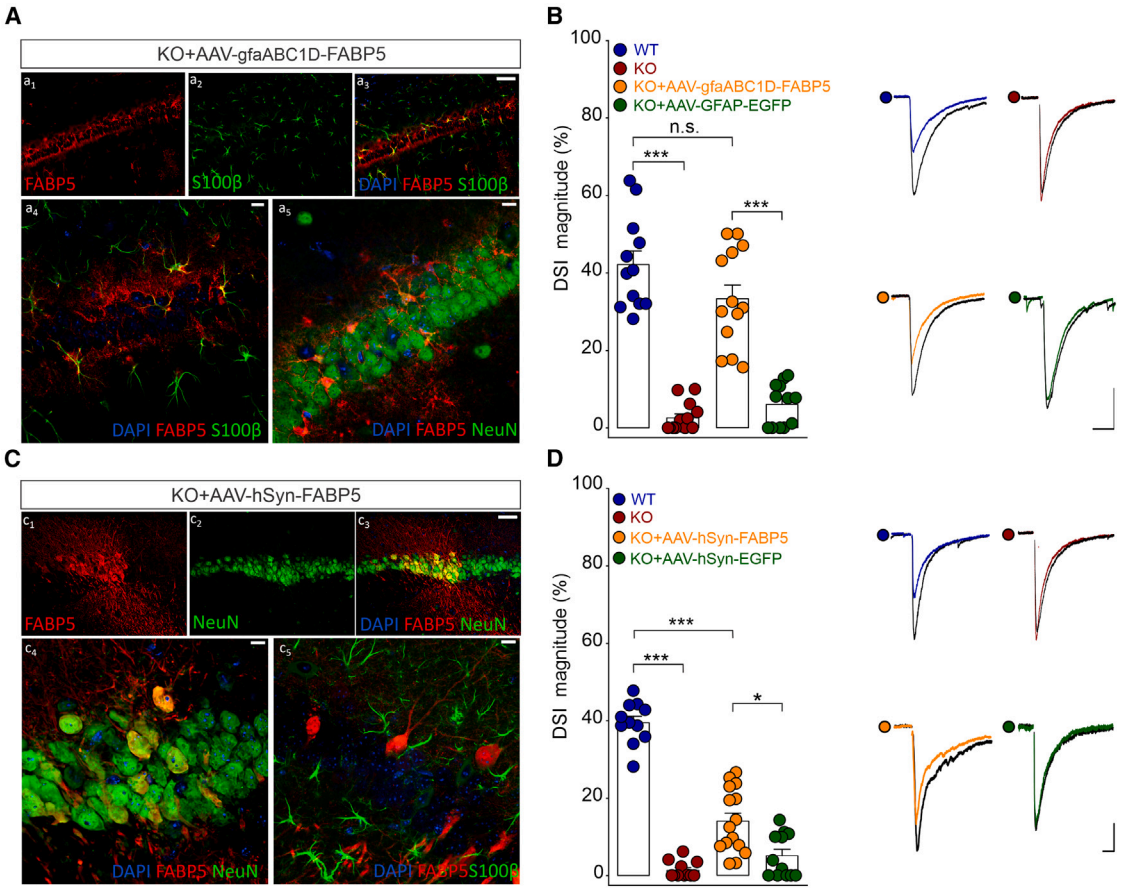

Figure 7. Expression of FABP5 in astrocytes of FABP5 KO mice rescues DSI

(A) AAV-mediated expression of FABP5 under the control of the gfaABC1D promoter in FABP5 KO mice. a1-a3, Immunostaining of FABP5, s100β and merge. Scale bar: 50 μm. a4, Co-localization of FABP5 with s100β. a5, Lack of co-localization of FABP5 with NeuN. Scale bars: 10 μm.

(B) Expression of FABP5 in astrocytes rescues DSI in FABP5 KO mice. Left panel, averaged magnitude of DSI obtained in WT (●: 42.23 ± 3.44%; $n = 12$ cells; $N = 3$ mice), KO (●: 2.65 ± 1.03%; $n = 13$ cells; $N = 3$ mice; $p = 3.28 \times 10^{-13}$ versus WT), KO+AAV-gfaABC1D-FABP5 (●: 33.37 ± 3.50%; $n = 13$ cells; $N = 4$ mice; $p = 0.12$ versus WT), and KO+AAV-GFAP-EGFP (●: 6.07 ± 1.58%; $n = 12$ cells; $N = 4$ mice; $p = 1.71 \times 10^{-8}$ versus KO+AAV-gfaABC1D-FABP5). Right panel, IPSC traces collected before and during DSI from WT (●), KO (●), KO+AAV-gfaABC1D-FABP5 (●), and KO+AAV-GFAP-EGFP (●). Scale bars: 100 ms, 200 pA.

(C) AAV-mediated expression of FABP5 under the neuron-specific hsynapsin1 promoter in FABP5 KO mice. c1-c3, Immunostaining for NeuN, FABP5, and merge. Scale bar: 50 μm. c4, Co-localization of FABP5 with NeuN. c5, Lack of co-localization of FABP5 with s100β. Scale bars: 10 μm.

(D) Expression of FABP5 in neurons partially rescues DSI in FABP5 KO mice. Left panel, Summary of DSI magnitude recorded from WT (●: 39.52 ± 1.65%; $n = 11$ cells; $N = 5$ mice), KO (●: 1.43 ± 0.66%; $n = 11$ cells; $N = 4$ mice; $p = 4.67 \times 10^{-18}$ versus WT), KO+AAV-hSyn-FABP5 (●: 13.95 ± 2.13%; $n = 15$ cells; $N = 5$ mice; $p = 4.47 \times 10^{-13}$ versus WT) and KO+AAV-hSyn-EGFP (●: 5.15 ± 1.61%; $n = 12$ cells; $N = 4$ mice; $p = 0.89$ versus KO). Right panel, IPSC traces collected before and during DSI. Data are represented as mean ± SEM. *$p < 0.05$; ***$p < 0.001$, one-way ANOVA with Bonferroni's multiple comparisons test.

DISCUSSION

Endocannabinoids are ubiquitous retrograde messengers that control synaptic transmission and plasticity throughout the mammalian brain. The mechanism(s) underlying synaptic eCB transport remains poorly defined, although several potential modes of 2-AG trafficking have been proposed.[24] We previously demonstrated that the well-established intracellular eCB carrier FABP5 undergoes secretion by astrocytes, localizes to synapses, and is indispensable for retrograde 2-AG signaling at both glutamatergic and GABAergic synapses in the dorsal Raphe nucleus and the striatum, respectively.[40,41] Employing a combination of cell-type specific molecular and physiological approaches, our current study establishes a paradigm wherein extracellular FABP5 of astrocytic origin mediates the delivery of 2-AG to presynaptic CB1Rs. This model is supported first by the finding that the conditional deletion of astrocytic FABP5 abolishes DSI, while its selective re-expression in the astrocytes of FABP5 KO mice restores DSI. Second, FABP5^{SEC} is sufficient to mediate retrograde 2-AG signaling. Additional support for this model stems from observations that FABP5 localizes within the astrocyte-neuron tripartite synapse,[40,47] indicating that FABP5 is ideally positioned to mediate the rapid synaptic transport of 2-AG that is essential for short-term and long-term synaptic plasticity.

A notable finding of our current and previous studies is that other brains expressed FABPs cannot compensate for the loss of FABP5 as evidenced by the collapse of retrograde 2-AG

signaling in FABP5 KO mice. This function of FABP5 is likely attributable to its ability to be secreted into the synaptic cleft while maintaining its ligand binding capacity. Consistent with this concept, the AAV-mediated expression of FABP7, which exhibits a high affinity for 2-AG but does not undergo secretion from astrocytes,[37,40,55] fails to rescue DSI in FABP5 KO mice. Interestingly, the engineered FABP7^{SEC} variant lost its ability to interact with 2-AG whereas this function was preserved in FABP5^{SEC}. This distinguishing feature enables FABP5 to coordinate eCB transport in both the cytosol and extracellular space.

Results from previous studies have suggested alternate mechanisms to account for retrograde eCB transport. Lupica and colleagues demonstrated that the activation of Sigma-1 receptors mediates cocaine-induced 2-AG release via extracellular vesicles.[57] Interestingly, FABP5 was identified as a component of the released extracellular vesicles, although the functional implications of this finding remain to be explored. More recently, Albarran et al. reported that retrograde 2-AG signaling requires postsynaptic synucleins and SNAREs, suggesting vesicular release of 2-AG from postsynaptic neurons.[58] Specifically, the authors reported that metabotropic receptor-driven eCB signaling was abolished in mice harboring a triple knockout of α, β, γ synucleins and following the inactivation of postsynaptic SNAREs using tetanus toxin. However, it is noteworthy that previous findings demonstrated that postsynaptic eCB release is independent of exocytosis.[9] Clearly, additional work will be required to reconcile these divergent findings. Taken together, distinct mechanisms have been proposed to account for postsynaptic 2-AG mobilization, and it is tempting to speculate that these processes may operate in concert with synaptic FABP5 to enable the rapid delivery of postsynaptic 2-AG to presynaptic CB1Rs.

In addition to eCBs, multiple neuroactive lipid species are implicated in fine-tuning synaptic function and plasticity.[59–61] For instance, results from a previous study have shown that lipoxygenase metabolites of arachidonic acid mediate short-term potentiation of excitation at mossy fiber CA3 glutamate synapses, an effect that directly opposes synaptic depression induced by 2-AG.[59] Interestingly, this synaptic response is independent of post-synaptic vesicular exocytosis,[59] suggesting that a distinct mechanism may underlie trafficking of lipoxygenase metabolites. It is noteworthy that FABP5 binds to arachidonic acid and a subset of lipoxygenase metabolites with high affinity,[62,63] raising the possibility that FABP5 may also regulate their synaptic transport. We recently demonstrated that FABPs bind to and are indispensable for hippocampal synaptic gating by the arachidonic acid metabolites epoxyeicosatrienoic acids.[64] These studies support the emerging model wherein brain FABPs orchestrate lipid signaling at central synapses by mediating their intracellular and synaptic transport.

Our current findings establish an indispensable role for astrocytic FABP5 in gating retrograde 2-AG signaling. While our results demonstrate that secreted FABP5 mediates 2-AG transport, the mechanism(s) underlying its release from astrocytes remains undefined. FABP5 secretion may involve a combination of previously proposed pathways (e.g., lysosomal or sirtuin-dependent release) or a yet to be identified mechanism(s). In addition, it is well established that eCBs are synthesized and released in an activity-dependent manner, and it is conceivable that FABP5 secretion may be governed by astrocytic activity. It also remains to be established whether FABP5 directly deposits eCBs on the presynaptic neuron membrane as reported for other ligands or whether binding to CB1R may confer additional targeting specificity. Future studies will be required to address these fundamental mechanistic questions.

Limitations of the study

In this study, we combined *ex vivo* electrophysiology with genetic and pharmacological approaches to investigate the role of FABP5 in eCB transport at GABA synapses. Our results provide invaluable insights into the crucial role of astrocytic FABP5 in controlling retrograde 2-AG signaling in the hippocampus. Extending these findings to additional brain regions will provide compelling evidence linking astrocytic FABP5 to eCB transport across diverse central synapses. While our data revealed that astrocytic FABP5 mediates retrograde 2-AG transport, it does not rule out the potential contribution of neuronal FABP5 in the translocation of eCBs and other bioactive lipids in distinct brain areas. Moreover, further studies are required to determine the biochemical mechanism(s) underlying FABP5 secretion from astrocytes. Lastly, the role of astrocytic FABP5 in controlling eCB-mediated behavioral outputs remains to be established. Addressing these outstanding questions will advance our understanding of the functional dynamics of astrocytic FABP5 in synaptic eCB signaling.

RESOURCE AVAILABILITY

Lead contact

Further information and requests for resources and reagents should be directed to and will be fulfilled by the Lead Contact, Samir Haj-Dahmane (sh38@buffalo.edu).

Materials availability

The constructs and FABP5^{FLOX} mice reported in this article are available from the lead contact upon request.

Data and code availability

- Data availability. The data that support the findings of this study are available from the lead contact upon reasonable request.
- Code availability. This article does not report original code.
- Any additional information required to reanalyze the data reported in this article is available from the lead contact upon request.

ACKNOWLEDGMENTS

The authors wish to thank Rob Rieger at the Stony Brook University Biological Mass Spectrometry Core for help with eCB quantification, Robert Blosser with the cell count analysis, and the SPARC for confocal imaging. This work was supported by NIH grants R01MH122461 (to MK and SHD), R21DA045863 (to MK and SHD), and T32AA007583 (to SO).

AUTHOR CONTRIBUTIONS

S.O. conducted the *in vitro* slice electrophysiology studies, including AAV injections. M.F. conducted the immunofluorescent staining experiments and AAV injections. K.S. conducted the immunofluorescent staining experiments. C.G. conducted cell culture and western blot experiments. S.T.G. performed qPCR experiments and processed samples for mass spectrometry. I.O. provided the FABP5 inhibitor. S.O., M.F., R.Y.S., M.K., and S.H-D. designed the

study, analyzed the data, and wrote the article. All authors contributed to the article and approved the submitted version.

DECLARATION OF INTERESTS

The authors declare that they have no conflict of interest with respect to this work.

STAR★METHODS

Detailed methods are provided in the online version of this paper and include the following:

- KEY RESOURCES TABLE
- EXPERIMENTAL MODELS AND STUDY PARTICIPANT DETAILS
  - Animals
- METHOD DETAILS
  - Stereotaxic surgeries and AAV injections
  - Tamoxifen treatment
  - Immunofluorescence staining
  - Ex-vivo electrophysiology
  - Whole-Cell recordings
  - Reverse Transcription-qPCR
  - FABP5 expression, purification, and binding studies
  - Quantification of tissue eCB levels
- QUANTIFICATION AND STATISTICAL ANALYSIS

SUPPLEMENTAL INFORMATION

Supplemental information can be found online at https://doi.org/10.1016/j.isci.2025.112342.

Received: December 11, 2024
Revised: February 19, 2025
Accepted: March 31, 2025
Published: April 2, 2025

REFERENCES

1. Katona, I., and Freund, T.F. (2012). Multiple functions of endocannabinoid signaling in the brain. Annu. Rev. Neurosci. *35*, 529–558. https://doi.org/10.1146/annurev-neuro-062111-150420.
2. Araque, A., Castillo, P.E., Manzoni, O.J., and Tonini, R. (2017). Synaptic functions of endocannabinoid signaling in health and disease. Neuropharmacology *124*, 13–24. https://doi.org/10.1016/j.neuropharm.2017.06.017.
3. Scheyer, A., Yasmin, F., Naskar, S., and Patel, S. (2023). Endocannabinoids at the synapse and beyond: implications for neuropsychiatric disease pathophysiology and treatment. Neuropsychopharmacology *48*, 37–53. https://doi.org/10.1038/s41386-022-01438-7.
4. Howlett, A.C., and Abood, M.E. (2017). CB(1) and CB(2) Receptor Pharmacology. Adv. Pharmacol. *80*, 169–206. https://doi.org/10.1016/bs.apha.2017.03.007.
5. Ryberg, E., Larsson, N., Sjögren, S., Hjorth, S., Hermansson, N.O., Leonova, J., Elebring, T., Nilsson, K., Drmota, T., and Greasley, P.J. (2007). The orphan receptor GPR55 is a novel cannabinoid receptor. Br. J. Pharmacol. *152*, 1092–1101. https://doi.org/10.1038/sj.bjp.0707460.
6. Oubraim, S., Wang, R., Hausknecht, K.A., Shen, R.Y., and Haj-Dahmane, S. (2021). Tonic Endocannabinoid Signaling Gates Synaptic Plasticity in Dorsal Raphe Nucleus Serotonin Neurons Through Peroxisome Proliferator-Activated Receptors. Front. Pharmacol. *12*, 691219. https://doi.org/10.3389/fphar.2021.691219.
7. Chavez, A.E., Chiu, C.Q., and Castillo, P.E. (2010). TRPV1 activation by endogenous anandamide triggers postsynaptic long-term depression in dentate gyrus. Nat. Neurosci. *13*, 1511–1518. https://doi.org/10.1038/nn.2684.
8. Wilson, R.I., Kunos, G., and Nicoll, R.A. (2001). Presynaptic specificity of endocannabinoid signaling in the hippocampus. Neuron *31*, 453–462. https://doi.org/10.1016/s0896-6273(01)00372-5.
9. Wilson, R.I., and Nicoll, R.A. (2001). Endogenous cannabinoids mediate retrograde signalling at hippocampal synapses. Nature *410*, 588–592. https://doi.org/10.1038/35069076.
10. Ohno-Shosaku, T., Maejima, T., and Kano, M. (2001). Endogenous cannabinoids mediate retrograde signals from depolarized postsynaptic neurons to presynaptic terminals. Neuron *29*, 729–738. https://doi.org/10.1016/s0896-6273(01)00247-1.
11. Tanimura, A., Yamazaki, M., Hashimotodani, Y., Uchigashima, M., Kawata, S., Abe, M., Kita, Y., Hashimoto, K., Shimizu, T., Watanabe, M., et al. (2010). The endocannabinoid 2-arachidonoylglycerol produced by diacylglycerol lipase alpha mediates retrograde suppression of synaptic transmission. Neuron *65*, 320–327. https://doi.org/10.1016/j.neuron.2010.01.021.
12. Gao, Y., Vasilyev, D.V., Goncalves, M.B., Howell, F.V., Hobbs, C., Reisenberg, M., Shen, R., Zhang, M.Y., Strassle, B.W., Lu, P., et al. (2010). Loss of retrograde endocannabinoid signaling and reduced adult neurogenesis in diacylglycerol lipase knock-out mice. J. Neurosci. *30*, 2017–2024. https://doi.org/10.1523/JNEUROSCI.5693-09.2010.
13. Hashimotodani, Y., Ohno-Shosaku, T., and Kano, M. (2007). Presynaptic monoacylglycerol lipase activity determines basal endocannabinoid tone and terminates retrograde endocannabinoid signaling in the hippocampus. J. Neurosci. *27*, 1211–1219. https://doi.org/10.1523/JNEUROSCI.4159-06.2007.
14. Viader, A., Blankman, J.L., Zhong, P., Liu, X., Schlosburg, J.E., Joslyn, C.M., Liu, Q.S., Tomarchio, A.J., Lichtman, A.H., Selley, D.E., et al. (2015). Metabolic Interplay between Astrocytes and Neurons Regulates Endocannabinoid Action. Cell Rep. *12*, 798–808. https://doi.org/10.1016/j.celrep.2015.06.075.
15. Dinh, T.P., Carpenter, D., Leslie, F.M., Freund, T.F., Katona, I., Sensi, S.L., Kathuria, S., and Piomelli, D. (2002). Brain monoglyceride lipase participating in endocannabinoid inactivation. Proc. Natl. Acad. Sci. USA *99*, 10819–10824. https://doi.org/10.1073/pnas.152334899.
16. Pan, B., Wang, W., Long, J.Z., Sun, D., Hillard, C.J., Cravatt, B.F., and Liu, Q.S. (2009). Blockade of 2-arachidonoylglycerol hydrolysis by selective monoacylglycerol lipase inhibitor 4-nitrophenyl 4-(dibenzo[d] [1,3]dioxol-5-yl(hydroxy)methyl)piperidine-1-carboxylate (JZL184) Enhances retrograde endocannabinoid signaling. J. Pharmacol. Exp. Ther. *331*, 591–597. https://doi.org/10.1124/jpet.109.158162.
17. Glaser, S.T., Kaczocha, M., and Deutsch, D.G. (2005). Anandamide transport: a critical review. Life Sci. *77*, 1584–1604. https://doi.org/10.1016/j.lfs.2005.05.007.
18. Hermann, A., Kaczocha, M., and Deutsch, D.G. (2006). 2-Arachidonoylglycerol (2-AG) membrane transport: history and outlook. AAPS J. *8*, E409–E412.
19. Kaczocha, M., Glaser, S.T., and Deutsch, D.G. (2009). Identification of intracellular carriers for the endocannabinoid anandamide. Proc. Natl. Acad. Sci. USA *106*, 6375–6380. https://doi.org/10.1073/pnas.0901515106.
20. Kaczocha, M., Lin, Q., Nelson, L.D., McKinney, M.K., Cravatt, B.F., London, E., and Deutsch, D.G. (2012). Anandamide externally added to lipid vesicles containing trapped fatty acid amide hydrolase (FAAH) is readily hydrolyzed in a sterol-modulated fashion. ACS Chem. Neurosci. *3*, 364–368. https://doi.org/10.1021/cn300001w.
21. Nicolussi, S., and Gertsch, J. (2015). Endocannabinoid transport revisited. Vitam. Horm. *98*, 441–485. https://doi.org/10.1016/bs.vh.2014.12.011.
22. Fowler, C.J. (2013). Transport of endocannabinoids across the plasma membrane and within the cell. FEBS J. *280*, 1895–1904. https://doi.org/10.1111/febs.12212.

23. Maccarrone, M., Dainese, E., and Oddi, S. (2010). Intracellular trafficking of anandamide: new concepts for signaling. Trends Biochem. Sci. *35*, 601–608. https://doi.org/10.1016/j.tibs.2010.05.008.

24. Kaczocha, M., and Haj-Dahmane, S. (2022). Mechanisms of endocannabinoid transport in the brain. Br. J. Pharmacol. *179*, 4300–4310. https://doi.org/10.1111/bph.15469.

25. Furuhashi, M., and Hotamisligil, G.S. (2008). Fatty acid-binding proteins: role in metabolic diseases and potential as drug targets. Nat. Rev. Drug Discov. *7*, 489–503. https://doi.org/10.1038/nrd2589.

26. Xu, B., Chen, L., Zhan, Y., Marquez, K.N.S., Zhuo, L., Qi, S., Zhu, J., He, Y., Chen, X., Zhang, H., et al. (2022). The Biological Functions and Regulatory Mechanisms of Fatty Acid Binding Protein 5 in Various Diseases. Front. Cell Dev. Biol. *10*, 857919. https://doi.org/10.3389/fcell.2022.857919.

27. Storch, J., and Thumser, A.E. (2000). The fatty acid transport function of fatty acid-binding proteins. Biochim. Biophys. Acta *1486*, 28–44.

28. Storch, J., and Thumser, A.E. (2010). Tissue-specific functions in the fatty acid-binding protein family. J. Biol. Chem. *285*, 32679–32683. https://doi.org/10.1074/jbc.R110.135210.

29. Vanderheyden, W.M., Lefton, M., Flores, C.C., Owada, Y., and Gerstner, J.R. (2022). Fabp7 Is Required for Normal Sleep Suppression and Anxiety-Associated Phenotype following Single-Prolonged Stress in Mice. Neuroglia *3*, 73–83. https://doi.org/10.3390/neuroglia3020005.

30. Matsumata, M., Sakayori, N., Maekawa, M., Owada, Y., Yoshikawa, T., and Osumi, N. (2012). The effects of fabp7 and fabp5 on postnatal hippocampal neurogenesis in the mouse. Stem Cell. *30*, 1532–1543. https://doi.org/10.1002/stem.1124.

31. Owada, Y., Yoshimoto, T., and Kondo, H. (1996). Spatio-temporally differential expression of genes for three members of fatty acid binding proteins in developing and mature rat brains. J. Chem. Neuroanat. *12*, 113–122. https://doi.org/10.1016/s0891-0618(96)00192-5.

32. Yamamoto, Y., Kida, H., Kagawa, Y., Yasumoto, Y., Miyazaki, H., Islam, A., Ogata, M., Yanagawa, Y., Mitsushima, D., Fukunaga, K., and Owada, Y. (2018). FABP3 in the Anterior Cingulate Cortex Modulates the Methylation Status of the Glutamic Acid Decarboxylase(67) Promoter Region. J. Neurosci. *38*, 10411–10423. https://doi.org/10.1523/JNEUROSCI.1285-18.2018.

33. Crofton, E.J., Nenov, M.N., Zhang, Y., Tapia, C.M., Donnelly, J., Koshy, S., Laezza, F., and Green, T.A. (2021). Topographic transcriptomics of the nucleus accumbens shell: Identification and validation of fatty acid binding protein 5 as target for cocaine addiction. Neuropharmacology *183*, 108398. https://doi.org/10.1016/j.neuropharm.2020.108398.

34. Yu, S., Levi, L., Casadesus, G., Kunos, G., and Noy, N. (2014). Fatty acid-binding protein 5 (FABP5) regulates cognitive function both by decreasing anandamide levels and by activating the nuclear receptor peroxisome proliferator-activated receptor beta/delta (PPARbeta/delta) in the brain. J. Biol. Chem. *289*, 12748–12758. https://doi.org/10.1074/jbc.M114.559062.

35. Berger, W.T., Ralph, B.P., Kaczocha, M., Sun, J., Balius, T.E., Rizzo, R.C., Haj-Dahmane, S., Ojima, I., and Deutsch, D.G. (2012). Targeting fatty acid binding protein (FABP) anandamide transporters - a novel strategy for development of anti-inflammatory and anti-nociceptive drugs. PLoS One *7*, e50968. https://doi.org/10.1371/journal.pone.0050968.

36. Kaczocha, M., Rebecchi, M.J., Ralph, B.P., Teng, Y.H.G., Berger, W.T., Galbavy, W., Elmes, M.W., Glaser, S.T., Wang, L., Rizzo, R.C., et al. (2014). Inhibition of fatty acid binding proteins elevates brain anandamide levels and produces analgesia. PLoS One *9*, e94200. https://doi.org/10.1371/journal.pone.0094200.

37. Sanson, B., Wang, T., Sun, J., Wang, L., Kaczocha, M., Ojima, I., Deutsch, D., and Li, H. (2014). Crystallographic study of FABP5 as an intracellular endocannabinoid transporter. Acta Crystallogr. D Biol. Crystallogr. *70*, 290–298. https://doi.org/10.1107/S1399004713026795.

38. Kaczocha, M., Vivieca, S., Sun, J., Glaser, S.T., and Deutsch, D.G. (2012). Fatty acid-binding proteins transport N-acylethanolamines to nuclear receptors and are targets of endocannabinoid transport inhibitors. J. Biol. Chem. *287*, 3415–3424. https://doi.org/10.1074/jbc.M111.304907.

39. Peng, X., Studholme, K., Kanjiya, M.P., Luk, J., Bogdan, D., Elmes, M.W., Carbonetti, G., Tong, S., Gary Teng, Y.H., Rizzo, R.C., et al. (2017). Fatty-acid-binding protein inhibition produces analgesic effects through peripheral and central mechanisms. Mol. Pain *13*, 1744806917697007. https://doi.org/10.1177/1744806917697007.

40. Haj-Dahmane, S., Shen, R.Y., Elmes, M.W., Studholme, K., Kanjiya, M.P., Bogdan, D., Thanos, P.K., Miyauchi, J.T., Tsirka, S.E., Deutsch, D.G., and Kaczocha, M. (2018). Fatty-acid-binding protein 5 controls retrograde endocannabinoid signaling at central glutamate synapses. Proc. Natl. Acad. Sci. USA *115*, 3482–3487. https://doi.org/10.1073/pnas.1721339115.

41. Fauzan, M., Oubraim, S., Yu, M., Glaser, S.T., Kaczocha, M., and Haj-Dahmane, S. (2022). Fatty Acid-Binding Protein 5 Modulates Brain Endocannabinoid Tone and Retrograde Signaling in the Striatum. Front. Cell. Neurosci. *16*, 936939. https://doi.org/10.3389/fncel.2022.936939.

42. Peng, H., Xin, S., Pfeiffer, S., Müller, C., Merl-Pham, J., Hauck, S.M., Harter, P.N., Spitzer, D., Devraj, K., Varynskyi, B., et al. (2024). Fatty acid-binding protein 5 is a functional biomarker and indicator of ferroptosis in cerebral hypoxia. Cell Death Dis. *15*, 286. https://doi.org/10.1038/s41419-024-06681-y.

43. Villeneuve, J., Bassaganyas, L., Lepreux, S., Chiritoiu, M., Costet, P., Ripoche, J., Malhotra, V., and Schekman, R. (2018). Unconventional secretion of FABP4 by endosomes and secretory lysosomes. J. Cell Biol. *217*, 649–665. https://doi.org/10.1083/jcb.201705047.

44. Josephrajan, A., Hertzel, A.V., Bohm, E.K., McBurney, M.W., Imai, S.I., Mashek, D.G., Kim, D.H., and Bernlohr, D.A. (2019). Unconventional Secretion of Adipocyte Fatty Acid Binding Protein 4 Is Mediated By Autophagic Proteins in a Sirtuin-1-Dependent Manner. Diabetes *68*, 1767–1777. https://doi.org/10.2337/db18-1367.

45. Guo, D., Lin, C., Lu, Y., Guan, H., Qi, W., Zhang, H., Shao, Y., Zeng, C., Zhang, R., Zhang, H., et al. (2022). FABP4 secreted by M1-polarized macrophages promotes synovitis and angiogenesis to exacerbate rheumatoid arthritis. Bone Res. *10*, 45. https://doi.org/10.1038/s41413-022-00211-2.

46. Fujita, K., Kume, H., Matsuzaki, K., Kawashima, A., Ujike, T., Nagahara, A., Uemura, M., Miyagawa, Y., Tomonaga, T., and Nonomura, N. (2017). Proteomic analysis of urinary extracellular vesicles from high Gleason score prostate cancer. Sci. Rep. *7*, 42961. https://doi.org/10.1038/srep42961.

47. Takano, T., Wallace, J.T., Baldwin, K.T., Purkey, A.M., Uezu, A., Courtland, J.L., Soderblom, E.J., Shimogori, T., Maness, P.F., Eroglu, C., and Soderling, S.H. (2020). Chemico-genetic discovery of astrocytic control of inhibition in vivo. Nature *588*, 296–302. https://doi.org/10.1038/s41586-020-2926-0.

48. Bogdan, D., Falcone, J., Kanjiya, M.P., Park, S.H., Carbonetti, G., Studholme, K., Gomez, M., Lu, Y., Elmes, M.W., Smietalo, N., et al. (2018). Fatty acid-binding protein 5 controls microsomal prostaglandin E synthase 1 (mPGES-1) induction during inflammation. J. Biol. Chem. *293*, 5295–5306. https://doi.org/10.1074/jbc.RA118.001593.

49. Bogdan, D.M., Studholme, K., DiBua, A., Gordon, C., Kanjiya, M.P., Yu, M., Puopolo, M., and Kaczocha, M. (2022). FABP5 deletion in nociceptors augments endocannabinoid signaling and suppresses TRPV1 sensitization and inflammatory pain. Sci. Rep. *12*, 9241. https://doi.org/10.1038/s41598-022-13284-0.

50. Gordon, C., Trainor, J., Shah, R.J., Studholme, K., Gelman, A., Doswell, F., Sadar, F., Giovannetti, A., Gershenson, J., Khan, A., et al. (2024). Fatty acid binding protein 5 inhibition attenuates pronociceptive cytokine/chemokine expression and suppresses osteoarthritis pain: A comparative human and rat study. Osteoarthr. Cartil. *32*, 266–280. https://doi.org/10.1016/j.joca.2023.11.010.

51. Hillowe, A., Gordon, C., Wang, L., Rizzo, R.C., Trotman, L.C., Ojima, I., Bialkowska, A., and Kaczocha, M. (2023). Fatty acid binding protein 5 regulates docetaxel sensitivity in taxane-resistant prostate cancer cells. PLoS One *18*, e0292483. https://doi.org/10.1371/journal.pone.0292483.

52. Yan, S., Elmes, M.W., Tong, S., Hu, K., Awwa, M., Teng, G.Y.H., Jing, Y., Freitag, M., Gan, Q., Clement, T., et al. (2018). SAR studies on truxillic acid mono esters as a new class of antinociceptive agents targeting fatty acid binding proteins. Eur. J. Med. Chem. *154*, 233–252. https://doi.org/10.1016/j.ejmech.2018.04.050.

53. Wang, H., Taouil, A., Awwa, M., Clement, T., Zhu, C., Kim, J., Rendina, D., Jayanetti, K., Maharaj, A., Wang, L., et al. (2022). SAR study on Novel truxillic acid monoester-Based inhibitors of fatty acid binding proteins as Next-Generation antinociceptive agents. Bioorg. Chem. *129*, 106184. https://doi.org/10.1016/j.bioorg.2022.106184.

54. Bao, Z., Malki, M.I., Forootan, S.S., Adamson, J., Forootan, F.S., Chen, D., Foster, C.S., Rudland, P.S., and Ke, Y. (2013). A novel cutaneous Fatty Acid-binding protein-related signaling pathway leading to malignant progression in prostate cancer cells. Genes Cancer *4*, 297–314. https://doi.org/10.1177/1947601913499155.

55. Elmes, M.W., Kaczocha, M., Berger, W.T., Leung, K., Ralph, B.P., Wang, L., Sweeney, J.M., Miyauchi, J.T., Tsirka, S.E., Ojima, I., and Deutsch, D.G. (2015). Fatty acid-binding proteins (FABPs) are intracellular carriers for Delta9-tetrahydrocannabinol (THC) and cannabidiol (CBD). J. Biol. Chem. *290*, 8711–8721. https://doi.org/10.1074/jbc.M114.618447.

56. Srinivasan, R., Lu, T.Y., Chai, H., Xu, J., Huang, B.S., Golshani, P., Coppola, G., and Khakh, B.S. (2016). New Transgenic Mouse Lines for Selectively Targeting Astrocytes and Studying Calcium Signals in Astrocyte Processes In Situ and In Vivo. Neuron *92*, 1181–1195. https://doi.org/10.1016/j.neuron.2016.11.030.

57. Nakamura, Y., Dryanovski, D.I., Kimura, Y., Jackson, S.N., Woods, A.S., Yasui, Y., Tsai, S.Y., Patel, S., Covey, D.P., Su, T.P., and Lupica, C.R. (2019). Cocaine-induced endocannabinoid signaling mediated by sigma-1 receptors and extracellular vesicle secretion. Elife *8*, e47209. https://doi.org/10.7554/eLife.47209.

58. Albarran, E., Sun, Y., Liu, Y., Raju, K., Dong, A., Li, Y., Wang, S., Südhof, T.C., and Ding, J.B. (2023). Postsynaptic synucleins mediate endocannabinoid signaling. Nat. Neurosci. *26*, 997–1007. https://doi.org/10.1038/s41593-023-01345-0.

59. Carta, M., Lanore, F., Rebola, N., Szabo, Z., Da Silva, S.V., Lourenço, J., Verraes, A., Nadler, A., Schultz, C., Blanchet, C., and Mulle, C. (2014). Membrane lipids tune synaptic transmission by direct modulation of presynaptic potassium channels. Neuron *81*, 787–799. https://doi.org/10.1016/j.neuron.2013.12.028.

60. Li, N., and Li, Y. (2024). Lysophosphatidic Acid (LPA) and Its Receptors in Mood Regulation: A Systematic Review of the Molecular Mechanisms and Therapeutic Potential. Int. J. Mol. Sci. *25*, 7440. https://doi.org/10.3390/ijms25137440.

61. Incontro, S., Musella, M.L., Sammari, M., Di Scala, C., Fantini, J., and Debanne, D. (2025). Lipids shape brain function through ion channel and receptor modulations: physiological mechanisms and clinical perspectives. Physiol. Rev. *105*, 137–207. https://doi.org/10.1152/physrev.00004.2024.

62. Xu, L.Z., Sánchez, R., Sali, A., and Heintz, N. (1996). Ligand specificity of brain lipid-binding protein. J. Biol. Chem. *271*, 24711–24719. https://doi.org/10.1074/jbc.271.40.24711.

63. Kane, C.D., Coe, N.R., Vanlandingham, B., Krieg, P., and Bernlohr, D.A. (1996). Expression, purification, and ligand-binding analysis of recombinant keratinocyte lipid-binding protein (MAL-1), an intracellular lipid-binding found overexpressed in neoplastic skin cells. Biochemistry *35*, 2894–2900. https://doi.org/10.1021/bi952476e.

64. Glaser, S.T., Jayanetti, K., Oubraim, S., Hillowe, A., Frank, E., Jong, J., Wang, L., Wang, H., Ojima, I., Haj-Dahmane, S., and Kaczocha, M. (2023). Fatty acid binding proteins are novel modulators of synaptic epoxyeicosatrienoic acid signaling in the brain. Sci. Rep. *13*, 15234. https://doi.org/10.1038/s41598-023-42504-4.

65. Maeda, K., Uysal, K.T., Makowski, L., Görgün, C.Z., Atsumi, G., Parker, R.A., Brüning, J., Hertzel, A.V., Bernlohr, D.A., and Hotamisligil, G.S. (2003). Role of the fatty acid binding protein mal1 in obesity and insulin resistance. Diabetes *52*, 300–307. https://doi.org/10.2337/diabetes.52.2.300.

66. Kaczocha, M., Glaser, S.T., Maher, T., Clavin, B., Hamilton, J., O'Rourke, J., Rebecchi, M., Puopolo, M., Owada, Y., and Thanos, P.K. (2015). Fatty acid binding protein deletion suppresses inflammatory pain through endocannabinoid/N-acylethanolamine-dependent mechanisms. Mol. Pain *11*, 52. https://doi.org/10.1186/s12990-015-0056-8.

STAR★METHODS

KEY RESOURCES TABLE

REAGENT or RESOURCE	SOURCE	IDENTIFIER
Antibodies		
Rabbit anti-FABP5	BioVendor R&D	RD181060100
Goat anti-FABP5	R&D Systems Inc	AF1476
Mouse anti-NeuN	Millipore	MAB377
Rabbit anti-NeuN	Abcam	AB104225
Mouse anti-s100β	Sigma-Aldrich	S2532
Alexa Fluor 594 donkey anti-rabbit	Jackson ImmunoResearch Labs	711-585-152 RRID: AB_2340621
Alexa Fluor 594 donkey anti-goat	Jackson ImmunoResearch Labs	711-585-152
Alexa Fluor 488 AffiniPure donkey anti-mouse IgG (H + L) antibody	Jackson ImmunoResearch Labs	715-545-151, RRID: AB_2341099
Alexa Fluor® 647 AffiniPure™ Donkey Anti-Rabbit IgG (H + L) antibody	Jackson ImmunoResearch Labs	711-605-152 RRID: AB_2492288
Alexa Fluor® 647 AffiniPure™ Donkey Anti-Mouse IgG (H + L) antibody	Jackson ImmunoResearch Labs	715-605-151 RRID: AB_2340863
Bacterial and virus strains		
AAV-CAG-FABP5 (serotype AAV9)	Duke VVC	pBK366
AAV-CAG-FABP5^{MUT} (serotype AAV9)	Duke VVC	pBK1937
AAV-CAG-FABP5^{SEC} (serotype AAV9)	Duke VVC	pBK383
AAV-CAG-FABP7 (serotype AAV9)	Duke VVC	pBK1433
AAV-CMV-Cre (serotype AAV9)	Addgene	105545
AAV-CMV-GFP (serotype AAV9)	Addgene	105530
AAV-hSyn-Cre (serotype AAV5)	Addgene	105540
pAAV-hSyn-EGFP (serotype AAV5)	Addgene	50465
AAV-gfaABC1D-FABP5 (serotype AAV8)	Duke VVC	pBK1762
pAAV.GFAP.eGFP.WPRE.hGH (serotype AAV5)	Addgene	105549
AAV-hSyn-FABP5 (serotype AAV5)	Duke VVC	pBK1761
Chemicals, peptides, and recombinant proteins		
NaCl	Fisher Scientific	CAS # 7647-14-5
Choline-Cl	Fisher Scientific	CAS # 1879-5008
CaCl2	Fisher Scientific	CAS # 10035-04-8
MgSO4	Fisher Scientific	CAS # 10034-99-8
KCl	Fisher Scientific	CAS # 7447-40-7
NaH2PO4	Fisher Scientific	CAS # 10049-21-5
NaHCO3	Fisher Scientific	CAS # 144-55-8
Glucose	Fisher Scientific	CAS # 50-99-7
Sodium L-ascorbate	Acros Organics	AC352685000
Sodium pyruvate	Sigma-Aldrich	CAS # 113-24-6
D-AP-5	Tocris	CAS# 79055-68-8
DNQX	Tocris	CAS# 1312992-24-7
Tamoxifen	Sigma-Aldrich	CAS# 10540-29-1
Corn oil	Sigma-Aldrich	CAS# 8001-30-7
WIN55,212-2	Tocris	CAS# 131543-23-2
SBFI-103	Yan et al. 2018[52]	
Internal standard for 2-AG-D5	Cayman	CAS# 2522598-88-3
Internal standard for AEA-D4	Cayman	CAS# 946524-40-9

(*Continued on next page*)

Continued

REAGENT or RESOURCE	SOURCE	IDENTIFIER
DAUDA probe	Cayman	CAS# 73025-02-2
ANS probe	Cayman	CAS# 82-76-8
2-AG	Cayman	CAS# 53847-30-6
AA	Cayman	CAS# 506-32-1
Critical commercial assays		
RNeasy Mini Kit	Qiagen	74104
Experimental models: Cell lines		
HEK-293 cells	ATCC	CRL-1573
Experimental models: Organisms/strains		
C57BL/6J mice	The Jackson Laboratory	JAX:000664
$FABP5^{FLOX}$-tdTomato mice	This paper	
FABP5 KO mice	Maeda et al. 2003[65]	Mal1 KO
Aldh1l1-Cre/ERT2 mice	The Jackson Laboratory	JAX:031008
Oligonucleotides		
See STAR Methods for the full sequence of primers	IDT	
Recombinant DNA		
pET28a	Novagen	#69864-3
pSecTag2/HygroC	Invitrogen	#V90020
Software and algorithms		
pClamp software	Molecular Devices	v10.7
Origin software	OriginLab Co	v 9.0
Clampfit software	Molecular Devices	v10.7
CorelDRAW Graphics Suite	Coreldraw.	v2019
Confocal AX-Elements imaging software	Nikon	v5.21
Prism software	GraphPad	v10
Other		
Vibrance antifade mounting medium with DAPI	Vectashield	H-1800
30 kDa MWCO ultrafiltration device	Corning Spin-X UF	431489
GenJet Plus Transfection Reagent	SignaGen	SL100499
Superscript III First Strand synthesis kit for Real-Time PCR	Invitrogen	11752–050
Taq DNA Polymerase with Standard Taq Buffer	NEB	M0273L
PowerUp SYBR Green Master Mix 5 × 5ml	Thermo Fisher	A25777
StepOnePlus PCR instrument	Applied Biosystems	4376600
Thermo TSQ Quantum Access Mass Spectrometer	Stony Brook Biological Mass Spectrometry Center	
33-gauge small hub RN needle, 15° bevel angle and syringe	Hamilton	REF # 65460-03
Homeothermic blanket control unit	Harvard apparatus	Item # 55-7020
KOPF instruments	Tujunga	https://kopfinstruments.com/
Stoelting pump	Stoelting Co	https://stoeltingco.com/
Vibratome Leica	Leica Biosystem	VT1200S
Olympus BX51 microscope	Molecular Devices	https://www.moleculardevices.com/
Multiclamp 700B amplifier	Molecular Devices	https://www.moleculardevices.com/
Digidata 1440	Molecular Devices	https://www.moleculardevices.com/
Microtome	American Optical	860 model

(*Continued on next page*)

Continued

REAGENT or RESOURCE	SOURCE	IDENTIFIER
Ti2E AXR Confocal Microscope	Nikon	https://www.microscope.healthcare.nikon.com/products/confocal-microscopes/ax
Thermo TSQ Quantum Access MAX Triple Quad LC/MS		https://gentechscientific.com/product/tsq-quantum-access-max/

EXPERIMENTAL MODELS AND STUDY PARTICIPANT DETAILS

Animals

All experimental procedures were approved by the Institutional Animal Care and Use Committees of Stony Brook University (#1486041) and University at Buffalo (#RIA01023N). Male and female (3–4 months old) C57BL/6J mice (Jackson Labs), FABP5^{Flox}, and FABP5 KO mice were group housed (3–4 per cage) with *ad libitum* access to food and water in a temperature-controlled environment and 12h light/12h dark cycles. Our FABP5^{FLOX} mice were generated by Cyagen. The FABP5 gene is located on chromosome 3 and contains four exons. The first *loxP* site was inserted into intron 1 while a cassette containing a *loxP* site followed by the endogenous splicing acceptor of intron 1, tdTomato, and an rBG polyA sequence was inserted ~500 base pairs downstream of exon 4. The targeting vector was co-injected with Cas9 and gRNA into fertilized eggs from C57Bl/6 mice. The resulting mice were further backcrossed onto C57Bl/6J mice (Jackson Labs).

METHOD DETAILS

Stereotaxic surgeries and AAV injections

Mice (5–6 weeks old) were anesthetized with 2.5% isoflurane in 100% oxygen and maintained in 1.5% isoflurane on a stereotaxic frame (KOFP instruments, Tujunga, CA). The head was shaved and the scalp was disinfected with iodine solution. A lubricant eye ointment was applied and the body temperature was controlled and maintained at 37°C–38°C using a homeothermic blanket control unit (Harvard apparatus). A small incision was made to expose the skull. The hippocampus coordinates (to bregma: AP, −2.5, ML, ±2, DV, −1.6 to brain surface) were used to mark and drill small holes through the skull. Bilateral injections of the virus (300 nL/side, 1x10^{12} titer/ml at a rate of 100 nL/min) were performed using a 33-gauge needle attached to a 5 μL syringe (Hamilton, Reno, NV) and driven by a Stoelting pump (Stoelting Co, Wood Dale, IL, USA). The virus was allowed to diffuse for 3 min before syringe removal. Mice were individually housed and observed for two days post-surgery. Electrophysiological recordings, immunostaining, and biochemical experiments were conducted at least three weeks after AAV injections.

The AAVs were custom generated at the Duke University Viral Vector Core or purchased from Addgene and utilized GFP to gauge transduction efficiency. The following AAVs were used: AAV-CAG-FABP5 expressing mouse FABP5 under the CAG promoter (Duke VVC #pBK366, serotype AAV9), AAV-CAG-FABP5^{MUT} expressing FABP5^{MUT} (Duke VVC #1937, serotype AAV9), AAV-CAG-FABP5^{SEC} expressing FABP5^{SEC} (Duke VVC #pBK383, serotype AAV9), AAV-CAG-FABP7 expressing mouse FABP7 (Duke VVC #pBK1433, serotype AAV9), AAV-CMV-Cre (Addgene, #105545, serotype AAV9), AAV-CMV-GFP (Addgene, #105530, serotype AAV9), AAV-hSyn-Cre (Addgene, #105540, serotype AAV5), pAAV-hSyn-EGFP (Addgene, #50465, serotype AAV5), AAV-gfaABC1D-FABP5 expressing FABP5 under the astrocyte-specific gfaABC1D promoter (Duke VVC #pBK1762, serotype AAV8), pAAV.GFAP.eGFP.WPRE.hGH (Addgene, #105549, serotype AAV5), and AAV-hSyn-FABP5 (Duke VVC #pBK1761, serotype AAV5).

Tamoxifen treatment

Tamoxifen (Sigma T5648, CAS Number: 10540-29-1) was dissolved in corn oil (Sigma C8267) and injected once daily for five consecutive days (75 mg/kg, i.p.). Control mice received injections of corn oil. The mice were euthanized at least three weeks later and brain tissues were processed for downstream experiments.

Immunofluorescence staining

Immunofluorescence was performed as described.[39] Hippocampal sections (30 μm) were incubated with the following primary antisera: rabbit anti-FABP5 (BioVendor R&D, RD181060100), goat anti-FABP5 (R&D Systems Inc, #AF1476), mouse anti-NeuN (Millipore, MAB377), rabbit anti-NeuN (Abcam, #AB104225), and mouse anti-s100β (Sigma, #S2532). Secondary antibodies used were Alexa Fluor 594 donkey anti-rabbit (Jackson ImmunoResearch Labs, #711-585-152, RRID: AB_2340621), Alexa Fluor 594 donkey anti-goat (Jackson ImmunoResearch Labs, #711-585-152), Alexa Fluor 488 AffiniPure donkey anti-mouse IgG (H + L) antibody (Jackson ImmunoResearch Labs, #715-545-151, RRID: AB_2341099), Alexa Fluor 647 AffiniPure Donkey Anti-Rabbit IgG (H + L) antibody (Jackson ImmunoResearch Labs, #711-605-152, RRID: AB_2492288), and Alexa Fluor 647 AffiniPure Donkey Anti-Mouse IgG (H + L) antibody (Jackson ImmunoResearch Labs, #715-605-151, RRID: AB_2340863). Fluorescent images were obtained using the Nikon Ti2E AXR Confocal Microscope and Confocal Nikon AX-Elements Imaging Software. Images were only adjusted for brightness and

contrast. FABP5 distribution in neurons and astrocytes was determined by counting all observed FABP5$^+$, NeuN$^+$, and s100β$^+$ cells from coronal hippocampal sections of WT mice. The percent distribution in astrocytes (FABP5$^+$/s100β$^+$ cells) and neurons (FABP5$^+$/NeuN$^+$) was calculated based on results obtained in six brain sections from two mice.

Ex-vivo electrophysiology

Brain Slices Preparation: Mice were deeply anesthetized with isoflurane and decapitated. The brain was rapidly removed and placed in a modified ice-cold chlorine-based artificial cerebrospinal fluid (ACSF) solution (Containing: 110 mM choline-Cl, 2.5 mM KCl, 0.5 mM $CaCl_2$, 7 mM $MgSO_2$, 1.25 mM NaH_2PO_4, 26.2 mM $NaHCO_3$, 11.6 mM sodium L-ascorbate, 3.1 mM sodium pyruvate, and 25 mM glucose) continuously bubbled with 95% O_2 and 5% CO_2. Coronal brain slices (350 μm thick) containing the hippocampus were prepared using a vibratome Leica VT 1200 (Leica, CA). The hippocampal slices were then incubated initially in a chamber containing the same cutting solution at 35°C for 15 min, followed by a transfer to a standard ACSF solution (Containing: 119 mM NaCl, 2.5 KCl, 2.5 mM $CaCl_2$, 1.3 mM $MgSO_4$, 1 mM NaH_2PO_4, 26.2 mM $NaHCO_3$, and 11 mM glucose) continuously bubbled with a mixture of 95% O_2 and 5% CO_2 for an additional 45 min at 35°C. Subsequently, the slices were recovered at room temperature for at least 30 min.

Whole-Cell recordings

Individual Hippocampal slices were transferred to a recording chamber, where they were continuously perfused with standard ACSF saturated with 95% O_2 and 5% CO_2 and maintained at 30°C for at least 15 min before recordings. CA1 pyramidal neurons were visualized using an upright microscope (BX 51 WI; Olympus, Tokyo, Japan), and somatic whole-cell recordings were performed from these neurons using glass pipette electrodes with 3–5 MΩ resistance when filled with an internal solution (Containing: 110 mM cesium gluconate, 10 mM CsCl, 10 mM Na2-phosphocreatine, 10 mM HEPES, 1 mM $MgCl_2$, 1 mM EGTA, 2 mM Na_2-ATP, 0.25 mM Na-GTP, 5 mM QX-314 chloride, pH 7.3 was adjusted with CsOH, osmolarity 280–290 mOsmol/l). All recordings were conducted in standard ACSF supplemented with 50 μM D-AP-5 and 20 μM DNQX to block NMDA and AMPA-mediated currents respectively. Inhibitory postsynaptic currents (IPSCs) were evoked with electrical pulses (5–20 V, 100–200 μs) delivered at 0.1 Hz using a glass microelectrode placed in the stratum radiatum in CA1 region of the hippocampus. To trigger depolarization-induced suppression of inhibition (DSI), IPSCs were evoked at 3-s intervals both before (3 IPSCs) and after (11 IPSCs) 10-s depolarization from −90 to 0 mV. All recorded currents were amplified with a Multiclamp 700B amplifier (Molecular Devices, Sunnyvale, CA), filtered at 3 kHz, digitized at 10 kHz with Digidata 1200 (Molecular Devices), and acquired using pClamp 10.7 software (Molecular Devices, Sunnyvale, CA).

Reverse Transcription-qPCR

RNA extractions were performed on hippocampal samples using the RNeasy Mini Kit (Qiagen) and cDNA was synthesized using the SuperScript III First-Strand Synthesis System (Thermo Fisher). The qPCR reaction was performed with PowerUp SYBR green (Thermo Fisher) on a StepOnePlus instrument (Applied Biosystems). Quantification was performed using the $2^{-\Delta\Delta Ct}$ method with β-Actin serving as the housekeeping gene. The following forward (F) and reverse (R) primers were used: CB1R: (F)AAGTCGATCTTAG ACGGCCTT and (R)TCCTAATTTGGATGCCATGTCTC; FAAH: (F)CCCTGCTCCAACTGGTACAG and (R)TCACAGTCAGTCAGATAG GAGG; MAGL: (F)CGGACTTCCAAGTTTTTGTCAGA and (R)GCAGCCACTAGGATGGAGATG; NAPE-PLD: (F)CTCCTGGACGACAA CAAGGTTC and (R)GCAAGGTCAAAAGGACCAAAC; ABHD4: (F)TTCCCCTACGACCAACTGAC and (R)CGAAGAACAGCCAGTGG ATT; ABHD6: (F)ACACAAGGACATGTGGCTCA and (R)ACTTGCCCCACTATGGACAG; DAGLα: (F)GTCCTGCCAGCTATCTTCCTC and (R)CGTGTGGGTTATAGACCAAGC; DAGLβ: (F)AGCGACGA CTTGGTGTTCC and (R)GCTGAGCAAGACTCCACCG; COX-2: (F)AGGACTGGGCCATGGAGT and (R)ACCTCTCCACCAATGACCTG; and β-Actin: (F)GACGGCCAGGTCATCACTAT and (R)CGGA TGTCAACGTCACACTT.

FABP5 expression, purification, and binding studies

Recombinant mouse FABP5, FABP5^{MUT}, and FABP7 were expressed with N-terminal His tags in *E. Coli* using the pET-28a vector (Novagen, Madison, WI, USA) and subsequently purified and delipidated as described.[35,52,53] FABP5^{SEC} and FABP7^{SEC} were generated by subcloning into the pSecTag2/Hygro C plasmid (Invitrogen) using *HindIII* and *XhoI*. The resulting proteins expressed an N-terminal signal peptide from Igk and C-terminal Myc and 6x-His tags. The constructs were transfected into HEK293T cells using GenJet Plus *In Vitro* DNA Transfection Reagent (SignaGen Laboratories, #SL100499). After 48h, culture media were collected and underwent centrifugation at 500*g* and 4°C to remove cellular debris. The media were then passed through 30 kDa molecular weight cut off ultrafiltration device (Corning Spin-X UF, #431489) and incubated with Ni-NTA agarose beads. Following two wash steps, purified FABP5 was eluted and subjected to FPLC size exclusion chromatography, delipidation, and concentration as described above. Protein purity was further confirmed by SDS-PAGE and Coomassie blue staining. Affinities of 2-AG and AA for purified FABP5, FABP5^{MUT}, and FABP5^{SEC} were quantified by assessing the displacement of the fluorescent 11-(dansylamino) undecanoic acid (DAUDA) probe from the FABP5 binding pocket as described.[52,53,64] Binding of 2-AG and AA to FABP7 and FABP7^{SEC} was determined using 8-anilinonaphthalene-1-sulfonic acid (ANS).[52,53,64] The fluorescence intensity values were normalized following background subtraction and fit to a one-site binding curve.

Quantification of tissue eCB levels

Mice were euthanized by rapid decapitation and hippocampal samples were rapidly excised and flash frozen in liquid nitrogen. Tissue levels of 2-AG and AEA were quantified using mass spectrometry-based lipidomics as described.[36,39,49,66] Briefly, the tissues were homogenized chloroform:methanol:Tris (2:1:1, pH) containing internal standards. Following centrifugation at 4°C, the organic layer was dried down with argon, resuspended in 2:1 chloroform:methanol and injected into the Thermo TSQ Quantum Access Triple Quadropole mass spectrometer. Liquid chromatography separation was achieved on a Gemini C18 column (50 × 2 mm × 5 μm) equipped with a Gemini C18 SecurityGuard precolumn (4 mm length x 2 mm internal diameter). Mobile phase A consisted of 95:5 water:methanol while mobile phase B was composed of 60:35:5 isopropanol:methanol:water and quantification was performed in the positive ion mode with 0.1% formic acid at a flow rate at 100 μL/min. The gradient started at 0% B and increased to 100% B over 15 min followed by an isocratic gradient of 100% B for 10 min and equilibration at 0% B for 15 min.

QUANTIFICATION AND STATISTICAL ANALYSIS

qPCR and eCB quantification were analyzed using unpaired t-tests. Electrophysiology data were analyzed using paired t-tests within-group comparisons and unpaired t-tests between groups with a significance threshold set at $p < 0.05$. To assess the effect of WIN55,212-2 (10 μM) (Tocris), the amplitude of IPSCs was normalized to the mean baseline amplitude recorded for 5 min before drug application. The amplitude of DSI was assessed as the percentage of the mean of three consecutive IPSCs amplitude immediately after membrane depolarization, relative to the average of the three before depolarization. The results are expressed as mean ± SEM. A parametric paired-t-test was used for within-group comparison. For comparison between groups, analysis of variance (ANOVA) with Bonferroni's multiple comparisons test was used. Statistical analyses were performed using Origin 9.0 software (MicroCal Software Inc, Northampton, MA, United States) and significance was set at $\alpha = 0.05$. Asterisks: $^{***}p < 0.001$, $^{**}p < 0.01$, $^{*}p < 0.05$.